On the Design of Broadbeam of Reconfigurable Intelligent Surface

Xinyi Lin, *Graduate Student Member, IEEE*, Lei Zhang, *Senior Member, IEEE*, Anvar Tukmanov, *Senior Member, IEEE*, Yihong Liu, *Graduate Student Member, IEEE*, Qammer Abbasi, *Senior Member, IEEE* and Muhammad Ali Imran, *Fellow Member, IEEE*

***Abstract*—Reconfigurable intelligent surface (RIS) has been identified as a promising disruptive innovation to realize a faster, safer and more efficient communication system. In this paper, we study the broad beamwidth design of RIS. A problem is formulated to achieve broadbeam with maximum and equal power gain within a pre-defined angular region given constraints of the unit modulus weights of RIS. Since the formulated problem is non-convex, where the optimal solution cannot be analytically obtained, we propose the difference-of-convex-based semi-definite programming (DC-SDP) algorithm. In addition, as important guidance of signal coverage for arbitrary angular regions, we mathematically derive the relationship between the angular range of the spatial sector and the maximum average received power. The upper bounds of the average received power with different RIS configurations are also obtained, where uniform rectangular array (URA) and uniform linear array (ULA) are considered. Simulation results demonstrate the effectiveness of our derivations and verify that our proposed DC-SDP algorithm is applicable in practical applications and outperforms other baseline methods. Overall, this work can be viewed as a foundation for the practical implementation of RIS on coverage enhancement and can also be seen as an initial step towards achieving channel estimation.**

***Index Terms*—Reconfigurable intelligent surface, broadbeam, beamforming, semi-definite programming, difference-of-convex.**

I. Introduction

Over the last decades, a quantum leap has been accomplished in the development of wireless communication. The emergence of various advanced techniques, including orthogonal frequency-division multiplexing (OFDM) [1], massive-multiple-input-multiple-output (M-MIMO) [2] and non-orthogonal multiple access (NOMA) [3], etc., has been witnessed. However, the main targets of the communication system remain unchanged, i.e. how to properly allocate scarce power and spectrum resources and meet the quality of service (QoS) requirements among users [4].

Recently, both academia and industry have begun to envision and project for the forthcoming 6^{th} generation (6G) technology, which will make up for the defects of the current communication system regarding the aforementioned targets. Specifically, some novel technologies such as Terahertz (THz) communication [5] and distributed radio access network (RAN) [6] are developed, which effectively improve communication efficiency. However, these technologies also mean huge hardware costs and energy consumption by deploying more active nodes and mounting more antennas [7]. Though capacity has been enhanced due to design on the precoder at the transmitter (Tx) side and/or the decoder at the receiver (Rx) side [8], optimization on the propagation environment has not been much explored yet. Indeed, it is the propagation environment that can significantly affect wireless transmission quality. In particular, the transmitted signals can be easily affected by blockages, extreme weather, etc., and thereby suffer from severe path loss and multipath fading. Hence, it is necessary to propose new paradigms that enable a significant reduction in hardware and energy costs, as well as a controllable and reconfigurable radio propagation environment.

Motivated by the aforementioned issues, a new and disruptive technology — reconfigurable intelligent surface (RIS), has been introduced and considered as a key enabling technology to realize challenging communication goals in the next few decades [9]. In particular, RIS is an artificial planar surface with sub-wavelength thickness leveraging a large number of passive scattering unit cell (UC) elements. Independent control of incident signals with reconfigurable amplitude and/or phase shifts could be realized on each element [10]. Then, the redirectional signals from all elements are combined and towards desired directions [11]. By densely deploying RISs and smartly coordinating them in wireless propagation environments, the reconfigurable and programmable end-to-end wireless channels could be eventually achieved [12].

Recent research advances have shown the application of RIS in various communication systems, such as RIS-aided NOMA system [13], RIS-aided secure transmission [14] , and RIS-aided cognitive radio (CR) system [15], etc. These works mainly focus on the design and optimization of active and passive beamforming under the assumption that the channel state information (CSI) is perfectly pre-known. However, to precisely assure system performance of all the above applications, channel estimation is definitely a core issue. In addition, channel estimation in RIS-assisted communication systems could be hard to achieve due to the passive property of RIS. Several works have been devoted to this topic. Specifically, a general framework for channel estimation in a RIS-aided

Manuscript submitted January 26, 2023, revised July 28, 2023, October 07, 2023, and December 05, 2023. The associate editor coordinating the review of this article was Amine Maaref. This work was supported in part by the U.K. Engineering and Physical Sciences Research Council (EPSRC) with British Telecom.

Xinyi Lin, Lei Zhang, Yihong Liu, Qammer Abbasi and Muhammad Ali Imran are all with the School of Engineering, University of Glasgow, G12 8QQ, U.K. (e-mail: x.lin.1@research.gla.ac.uk; Lei.Zhang@glasgow.ac.uk; y.liu.6@research.gla.ac.uk; Qammer.Abbasi@glasgow.ac.uk; Muhammad.Imran@glasgow.ac.uk).

Anvar Tukmanov is with British Telecommunications PLC, Adastral Park, Ipswich, U.K. (e-mail: anvar.tukmanov@bt.com).

system was introduced in [16] by leveraging a combined bilinear spare matrix factorization and matrix completion. This design is enabled by activating elements one by one at each stage of estimation and could therefore lead to poor real-time performance and large estimation variance. Following this work, the authors in [17] designed an optimal channel estimation scheme which is guided by results for the minimum variance unbiased estimation. It is proved that this work effectively reduces estimation variance. However, the pilot overhead could be extremely high when the size of RIS is large.

Since it is a challenge of channel estimation, recent research has investigated RIS-aided systems with incomplete CSI [18]. For example, the authors in [19] proposed a RIS phase shift design based on the statistical CSI and the formulated upper bound of the ergodic spectral efficiency. Additionally, a MISO system deploying distributed RISs was investigated in [20], where the achievable rate of the network was analyzed considering the CSI estimation error. Furthermore, a RIS-assisted anti-jamming communication scenario was proposed in [21]. Specifically, a robust RIS beamforming design is formulated to enhance the security performance with or without imperfect jammer's CSI.

In addition to the above works, some research has been devoted to the study of broadbeam, which is promising for avoiding the thorny problems that can be encountered in channel estimation. Specifically, as a low-cost and passive device, it is more realistic to use RIS to generate broadbeam, which could cover an angular region instead of locating users with real-time beam tracking or CSI. In addition, broadbeam design is also rewarding and beneficial for coverage enhancement. Furthermore, the design and implementation of the broadbeam can be simpler compared to the narrow-beam antenna system, as there is no need to steer the beam towards a specific direction precisely. This can lead to reduced complexity and much lower cost and henceforth, is more suitable to be deployed in practice. Specifically, in broadbeam design, the average received power and variance are generally considered as two critical metrics to measure the designed system. On one side, the average received power reflects the average QoS of all users in a specific area; the variance of the beam pattern, on the other side, validates the communication stability for users in movements.

To the best of our knowledge, there are only a few works investigating broadbeam design via RIS so far. For example, the authors in [22] proposed a RIS-aided downlink transmission where the reflection link is used to illuminate the area centred around the mobile user (MU). However, they only focused on the cover area but not the flatness of the generated beam pattern, which may lead to unstable data transmission. Motivated by this fact, the authors in [23] proposed a novel 3D beam broadening and flattening technique on an aerial intelligent reflecting surface (AIRS), where the AIRS is divided into several sub-arrays. By synthesizing the beams generated by each sub-array, a broad and flat beam could be achieved. However, the beamwidth could be restricted, especially when a small RIS is applied. In [24], a design framework to synthesize the power pattern reflected by the RIS was proposed, which meets the customized requirements of broad coverage and considers the flatness of the generated beams. An arbitrarily defined beamwidth at the RIS could be realized. However, the flat broadbeam is realized by minimizing the difference between the target pattern and the optimized pattern, where the average received power and variance of the beam pattern were not investigated.

To address the aforementioned issues, the blind coverage enhancement design is proposed in this paper, where signals with comparable received power are received by users at arbitrary places in a pre-defined sector area without knowing their precise directions. The average received power is maximized within the sector area. We illustrate the utility and superiority of our design for the following several reasons. Firstly, in this broadbeam-enhanced area coverage way, where a flat broadbeam is generated to cover a whole range instead of one specific user, the issue caused by the user's position changes can be solved well. Besides, RIS with the flat broadbeam design is not required to respond in real-time to users' movements, which could largely reduce the hardware cost as well as computational complexity. Furthermore, the possible active area of users is generally pre-known; the increase in signal-to-noise ratio (SNR) and the improvement in QoS could be enhanced by proposing the pre-defined area coverage enhancement design. Additionally, the SNR is further improved by maximizing the signals' received power within the pre-defined area.

In summary, the flat broadbeam design is well-suited for various applications, such as cellular communication, satellite broadcasting, and Wi-Fi networks, where wide coverage and robust performance are essential. Besides, the role of this design in establishing connections between RIS and users can be regarded as an initial step for other channel estimation algorithms. The main contributions are summarized as follows:

- We propose a design framework to generate broadbeam with a flattened top and maximized average received power within a pre-defined sector area. The flat broadbeam ensures the maximum sum rate compared with other beam patterns, which is numerically proved in this paper.
- As an important metric to measure QoS, the relationship between the average received power and the phase shifts of RIS is analytically obtained. Specifically, we obtain the upper bound of the average received power given RIS under both uniform rectangular array (URA) and uniform linear array (ULA) configurations.
- Difference-of-convex-based semi-definite programming (DC-SDP) algorithm is introduced in this paper, which effectively transfers the original non-convex problem into a convex form and realizes iterative rank reduction (IRR). We compare the simulation results using the DC-SDP algorithm with other baseline methods, and also with the cases when the RIS is randomly designed or when no RIS is applied. It is worth mentioning that the DC-SDP algorithm could always result in broadbeam with fewer fluctuations.

The remainder of the paper is organized as follows. Section II presents our system model and proposes the problem

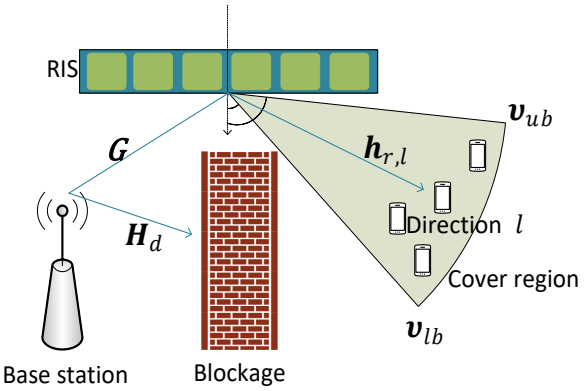

Fig. 1: System model of RIS-aided flat broadbeam design.

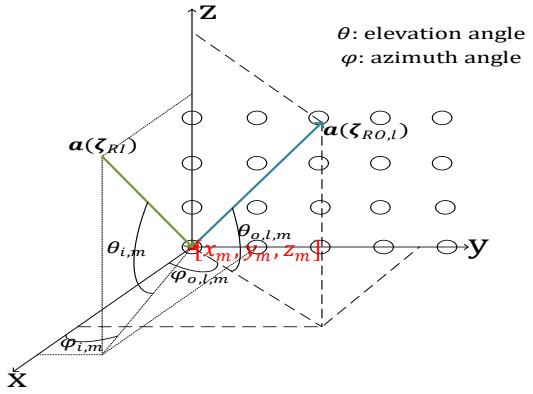

Fig. 2: 2D RIS under URA configuration in 3D geometry axis.

formulation on beam coverage regarding the RIS phase shifts design. Section III gives analytical derivations on average received power. Section IV introduces the DC-SDP optimization approach. Simulation results are presented in Section V. And the conclusion is drawn in Section VI.

Notations: Scalars, vectors, and matrices are denoted by lower-case, bold-face lower-case, and bold-face upper-case letters, respectively. $\mathbb{E}\{\cdot\}$ denotes the expectation value. $(\cdot)^T$, $(\cdot)^H$, and $(\cdot)^*$ represent the transpose, the conjugate transpose, and the conjugate of a vector, respectively. $\odot$ denotes the point-wise multiplication. $\|\boldsymbol{a}\|$ denotes the Euclidean norm of vector $\boldsymbol{a}$. $\text{rank}(\boldsymbol{A})$ and $\text{Tr}(\boldsymbol{A})$ denote the rank and trace of matrix $\boldsymbol{A}$, respectively. And $\text{Diag}(\boldsymbol{A})$ stands for a vector with elements defined by the diagonal entries of $\boldsymbol{A}$. Likewise, $\text{diag}(\boldsymbol{a})$ denotes a square matrix where $\boldsymbol{a}$ is positioned on the diagonal. $\mathbf{1}_M$ represents an $M\times 1$ identity vector. $\angle(\boldsymbol{a}) \in \mathbb{C}^{M\times 1}$ is the phase of the $M \times 1$ vector $\boldsymbol{a}$. $\partial\|\boldsymbol{A}\|_2$ denotes the sub-gradient of matrix $\boldsymbol{A}$. $Re\{\cdot\}$ and $Im\{\cdot\}$ stand for the real and imaginary parts of a complex number, respectively. And $\inf(S)$ and $\sup(S)$ represent the infimum and supremum of a subset S. Finally, we define domain $f = \{p \in P : f(p) < +\infty\}$ and we use $\langle \mathbf{Y}, \mathbf{Z} \rangle$ to refer to the inner product of two matrices.

II. System Model and Problem Formulation

A. Signal & Channel Model

We model a RIS-aided downlink system[1] as illustrated in Fig. 1. L random directions are chosen within the pre-defined area, which is constrained by $\varphi_{\{lb,ub\}}$ and $\theta_{\{lb,ub\}}$. Specifically, $\varphi_{\{lb,ub\}}$ and $\theta_{\{lb,ub\}}$ refer to horizontal and vertical lower and upper boundary angles of the cover region. We sequentially integrate $\boldsymbol{v}_{lb} = [\varphi_{lb}, \theta_{lb}]$ and $\boldsymbol{v}_{ub} = [\varphi_{ub}, \theta_{ub}]$. The BS is implemented with N antennas. And the proposed RIS contains M reflecting elements. In addition, users with a single antenna are assumed in this paper. Reflective links $\boldsymbol{h}_{r,l} \in \mathbb{C}^{M\times 1}, \forall l \in L$ are built to assist the BS in transmitting signals to multiple users within a sector area. Moreover, the BS-RIS and BS-user channels are denoted as $\boldsymbol{G} \in \mathbb{C}^{M\times N}$ and $\boldsymbol{H}_d = [\boldsymbol{h}_{d,1}, \cdots, \boldsymbol{h}_{d,l}, \cdots, \boldsymbol{h}_{d,L}] \in \mathbb{C}^{N\times L}$, respectively. We assume that the system works on the sub-6 GHz frequency band. The direct link $\boldsymbol{h}_{d,l}$ follows Rayleigh fading, while RIS-aided channels $\boldsymbol{h}_{r,l}$ and $\boldsymbol{G}$ follow Rician fading. Then, these channels are modelled as

$$\boldsymbol{h}_{d,l} = \text{PL}_{\text{NLoS}}\overline{\boldsymbol{h}}_{d,l}, \tag{1}$$

$$\boldsymbol{h}_{r,l} = \text{PL}_{\text{LoS},l}\left(\sqrt{\frac{\varepsilon}{\varepsilon+1}}\boldsymbol{a}(\zeta_{RO,l}) + \sqrt{\frac{1}{\varepsilon+1}}\overline{\boldsymbol{h}}_{r,l}\right), \tag{2}$$

$$\boldsymbol{G} = \text{PL}_{\text{LoS},0}\left(\sqrt{\frac{\varepsilon}{\varepsilon+1}}\boldsymbol{a}(\zeta_{RI})\boldsymbol{a}^H(\zeta_{BS}) + \sqrt{\frac{1}{\varepsilon+1}}\overline{\boldsymbol{G}}\right). \tag{3}$$

Specifically, PL_{NLoS}, $\text{PL}_{\text{LoS},l}$ and $\text{PL}_{\text{LoS},0}$ denote the corresponding path-loss. ε is the Rician factor. $\overline{\boldsymbol{h}}_{d,l}$, $\overline{\boldsymbol{h}}_{r,l}$, and $\overline{\boldsymbol{G}}$ denote the non-line-of-sight (NLoS) components of channels, each element of which follows $\mathcal{CN}(0,1)$. In addition, $\boldsymbol{a}(\zeta)$ denotes the steering vector as a function of the spatial information ζ [25], which is represented as

$$\boldsymbol{a}(\zeta) = e^{j\frac{2\pi d}{\lambda}\zeta}. \tag{4}$$

Note that ζ can follow either ULA or URA configuration. Moreover, $\zeta_{RO,l}$, ζ_{RI}, and ζ_{BS} are the functions of angles of departure (AoD) towards the user at the l-th direction, angles of arrival (AoA) at RIS and AoD at BS towards RIS, respectively. Specifically, we consider the URA configuration for both BS and RIS in our proposed system, then $\zeta_{RO,l}$, ζ_{RI}, and ζ_{BS} can be generalized as $\zeta = f(\varphi, \theta)$, where φ and θ refer to the azimuth and elevation angle, respectively. Fig. 2 shows the RIS model under URA configuration. Assume that there are M_y elements along the Y-axis and M_z elements along the Z-axis, then we have $M = M_y M_z$. In addition, we denote the azimuth angle $\varphi_{i,m}$ and elevation angle $\theta_{i,m}$ as the incident angles at the m-th element, and $\varphi_{o,l,m}$ and $\theta_{o,l,m}$ as the azimuth and elevation reflection angles at the m-th element in RIS. Note that m has a relationship with m_y and m_z as $m = (m_y - 1)M_z + m_z$, where $m_y \in \{1, \cdots, M_y\}$, $m_z \in \{1, \cdots, M_z\}$. The angle information $\zeta_{RI,m}$ and $\zeta_{RO,l,m}$ at the m-th element could be sequentially represented as

$$\zeta_{RI,m} = (m_y - 1)\cos\theta_{i,m}\sin\varphi_{i,m} + (m_z - 1)\sin\theta_{i,m}, \tag{5}$$

$$\zeta_{RO,l,m} = (m_y - 1)\cos\theta_{o,l,m}\sin\varphi_{o,l,m} + (m_z - 1)\sin\theta_{o,l,m}. \tag{6}$$

Similarly, the BS is modelled under the URA configuration on the x-y plane. We assume N_x elements along the X-axis and

[1]The system model is presented in 2D for simplicity, which can be easily extended to the general 3D model.

N_y elements along the Y-axis, where $N = N_x N_y$. φ_n and θ_n denote the azimuth and elevation angles from the n-th element of BS, respectively. The angle spatial information $\zeta_{BS,n}$ at the n-th element can be expressed as

$$\zeta_{BS,n} = (n_x - 1)\cos\theta_n \cos\varphi_n + (n_y - 1)\cos\theta_n \sin\varphi_n, \quad (7)$$

where $n = (n_x - 1)N_y + n_y$, $n_x \in \{1, \cdots, N_x\}$, $n_y \in \{1, \cdots, N_y\}$.

Let $\mathbf{w} = [w_1, w_2, ..., w_M]^H$ denotes the weight matrix of the RIS and each element $w_m, m = 1, 2, ..., M$ could be expressed as $w_m = \beta_m e^{j\alpha_m}$. For maximum reflecting efficiency, we let $\beta_m = 1$ and $\alpha_m \in [0, 2\pi]$. And the transmit beamforming vector at BS is $\boldsymbol{b} \in \mathbb{C}^{N\times 1}$. Then, the received signal at the l-th direction could be expressed as

$$y_l = (\boldsymbol{h}_{d,l}^H + \boldsymbol{h}_{r,l}^H \boldsymbol{W}\boldsymbol{G})\boldsymbol{b}\sqrt{p_t}s + n_l, \ \forall l \in L, \quad (8)$$

where $\boldsymbol{W} = \mathrm{diag}(\mathbf{w}^T) \in \mathbb{C}^{M\times M}$ and n_l is the additive white Gaussian noise (AWGN) with zero mean and variance σ_n^2, i.e., $n_l \sim \mathcal{CN}(0, \sigma_n^2)$. Additionally, p_t denotes the transmit power at the BS. Therefore, the received power at the l-th direction could be expressed as

$$p_l = |(\boldsymbol{h}_{d,l}^H + \boldsymbol{h}_{r,l}^H \boldsymbol{W}\boldsymbol{G})\boldsymbol{b}|^2 p_t + \sigma_n^2, \ \forall l \in L. \quad (9)$$

Based on the expression of the received power at the l-th direction, we formulate the optimization problem in the following subsection.

B. Optimization Problem

We propose the novel design of a perfect flat broadbeam with equal received power at all directions within the pre-defined cover region, which could be interpreted as

$$\begin{aligned} \text{(P1):} \quad \max_{\mathbf{w}} \quad & \Xi \\ \text{s.t.} \quad & p_l = \Xi, \ l \in L \\ & |w_m| = 1, \ m = 1, \cdots, M, \end{aligned} \quad (10)$$

where Ξ is defined as the average received power within the cover region. By solving (P1), a broadbeam with a flattened top and maximized average received power could be realized given the RIS unit modulus weights constraints.

By proposing the flat broadbeam design, users' received power can always be guaranteed without knowing their precise directions, and beam tracking is not required. Additionally, the investigation of flat broadbeam is crucial to realize the maximum sum rate, which enables the same received power along all directions. Specifically, based on the expression of the received power, the SNR for the user at the l-th direction could be expressed as

$$\mathrm{SNR}_l = \frac{|(\boldsymbol{h}_{d,l}^H + \boldsymbol{h}_{r,l}^H \boldsymbol{W}\boldsymbol{G})\boldsymbol{b}|^2 p_t}{\sigma_n^2}, \ \forall l \in L. \quad (11)$$

Sequentially, we represent the sum-rate of the chosen L directions between the cover range $\boldsymbol{\upsilon}_{lb}$ and $\boldsymbol{\upsilon}_{ub}$ as

$$R_{total} = \sum_{l=1}^{L} \log_2(1 + \mathrm{SNR}_l). \quad (12)$$

Moreover, we assume that the total received power of all directions within the cover region $[\boldsymbol{\upsilon}_{lb}, \boldsymbol{\upsilon}_{ub}]$ is denoted as P_{total}, which could be represented as

$$P_{total} = \sum_{l=1}^{L} (|(\boldsymbol{h}_{d,l}^H + \boldsymbol{h}_{r,l}^H \boldsymbol{W}\boldsymbol{G})\boldsymbol{b}|^2 p_t + \sigma_n^2). \quad (13)$$

Note that L should be sufficiently large to approximate that the received power at an arbitrary direction within the cover region $[\boldsymbol{\upsilon}_{lb}, \boldsymbol{\upsilon}_{ub}]$ equals the average received power. We further rewrite (12) as

$$R_{total} = \log_2(\prod_{l=1}^{L}(1 + \mathrm{SNR}_l)). \quad (14)$$

According to the Cauchy–Schwarz inequality [26], the following lemma can be derived.

Lemma 1: *For several variables denoted as $x_1, \cdots, x_N$ with fixed sum value, i.e., $x = x_1 + \cdots + x_N$, the maximum multiplication result can be achieved when and only when $x_1 = \cdots = x_N$.*

Based on **Lemma 1**, we can safely draw the conclusion that the maximum sum rate could be realized when

$$p_l = \Xi, \ l \in L. \quad (15)$$

In detail, the maximum sum rate can be realized when signals with the same received power are received by all directions within the pre-defined cover region.

III. Analysis on average received power

In order to evaluate the average received power within a pre-defined angular region, which is considered as an important metric to measure the performance of communications, some characteristics of the maximum average power based on the cover area are proposed in this section. Besides, an upper bound of the maximum average received power is derived for an arbitrary cover region.

We consider BS applying maximum ratio transmission (MRT) for maximal power transmission towards RIS, as the direct link suffers from serious channel fading and comprises only NLoS paths. Then we have $\boldsymbol{b} = \boldsymbol{a}^*(\boldsymbol{\zeta}_{BS})$. Moreover, the unit transmit power is assumed at the BS. Sequentially, the received power at the l-th direction [2] can be approximated as

$$p_l \approx |\boldsymbol{a}^H(\boldsymbol{\zeta}_{RO,l})\boldsymbol{W}\boldsymbol{a}(\boldsymbol{\zeta}_{RI})|^2, \ \forall l \in L. \quad (16)$$

By applying the change of variables $\boldsymbol{\gamma}_l = \boldsymbol{a}(\boldsymbol{\zeta}_{RO,l}) \odot \boldsymbol{a}(\boldsymbol{\zeta}_{RI}) \in \mathbb{C}^{M\times 1}$, we reformulate (16) as

$$p_l = |\mathbf{w}^H \boldsymbol{\gamma}_l|^2, \ \forall l \in L. \quad (17)$$

We further define $\boldsymbol{Q}_l = \boldsymbol{\gamma}_l \boldsymbol{\gamma}_l^H \in \mathbb{C}^{M\times M}$, then (17) is equivalent to

$$p_l = \mathbf{w}^H \boldsymbol{Q}_l \mathbf{w}, \quad (18)$$

which can be transformed as $\mathbf{w}^H \boldsymbol{Q}_l \mathbf{w} = \mathrm{Tr}(\boldsymbol{Q}_l \mathbf{w}\mathbf{w}^H), \forall l \in L$. The matrix lifting technique [27] is used to lift the original vector $\mathbf{w}$ as a positive semi-definite (PSD) matrix $\mathbf{X}$, which

[2] To be noted that in the subsequent derivation, we omit the noise in the expression of the received power, as the noise power is usually very low and will not affect the flatness of the generate beam over time scale.

equals the multiplication of $\mathbf{w}$ and its corresponding conjugate transpose, i.e., $\boldsymbol{X} = \mathbf{w}\mathbf{w}^H$, where $\text{rank}(\boldsymbol{X}) = 1$ and $\boldsymbol{X} \succeq 0$. Given $|w_m| = 1, m = 1, 2, ..., M$, $\boldsymbol{X}$ has to additionally satisfy $\text{Diag}(\boldsymbol{X}) = \mathbf{1}_M$. Then, the expression for p_l can be equivalently reformulated as

$$p_l = \text{Tr}(\boldsymbol{Q}_l \boldsymbol{X}), \ \forall l \in L. \tag{19}$$

In terms of (19), the average received power in all directions could be expressed as

$$\Xi = \mathbb{E}\{\text{Tr}(\boldsymbol{Q}_l \boldsymbol{X})\}, \ l \in L, \tag{20}$$

where $\boldsymbol{X}$ is the PSD matrix of RIS phase shifts, which is independent of received direction and can be fixed once RIS phase shifts are all determined. Then, (20) can be equivalently written as

$$\Xi = \text{Tr}(\mathbb{E}\{\boldsymbol{Q}_l\}\boldsymbol{X}), \ l \in L. \tag{21}$$

We expand the expression of γ_l as

$$\gamma_l = [\gamma_{l,11}, \cdots, \gamma_{l,1M_z}, \cdots, \gamma_{l,p_y p_z}, \cdots, \gamma_{l,M_y M_z}], \tag{22}$$

where $p_y = 1, \cdots, M_y$ and $p_z = 1, \cdots, M_z$. Similarly, we have $q_y = 1, \cdots, M_y$ and $q_z = 1, \cdots, M_z$. Then $\boldsymbol{Q}_l$ can be expressed as (23), which is shown on the top of the next page.

We denote $\mathbb{E}\{\boldsymbol{Q}_l\}$ as $\boldsymbol{\Upsilon} \in \mathbb{C}^{M \times M}$, then the average received power could be expressed as

$$\begin{aligned}\Xi = \ & \underbrace{\boldsymbol{\Upsilon}(1,1)\boldsymbol{X}(1,1) + \cdots, +\boldsymbol{\Upsilon}(1,M)\boldsymbol{X}(M,1)}_{M} + \underbrace{\cdots}_{M(M-2)} \\ & + \underbrace{\boldsymbol{\Upsilon}(M,1)\boldsymbol{X}(1,M) + \cdots, \boldsymbol{\Upsilon}(M,M)\boldsymbol{X}(M,M)}_{M}.\end{aligned} \tag{24}$$

Both $\boldsymbol{\Upsilon}$ and $\boldsymbol{X}$ are Hermitian matrices, we can henceforth derive that

$$\boldsymbol{\Upsilon}(p,q)\boldsymbol{X}(q,p) + \boldsymbol{\Upsilon}(q,p)\boldsymbol{X}(p,q) = 2Re\{\boldsymbol{\Upsilon}(p,q)\boldsymbol{X}(q,p)\}, \tag{25}$$

where both p and $q = 1, \cdots, M$. Note that p_y/q_y and p_z/q_z contain the placement information of the p/q-th elements in RIS. The average received power could be reformulated as

$$\Xi = 2\sum_{p=1}^{M}\sum_{q=p+1}^{M} Re\{\boldsymbol{\Upsilon}(p,q)\boldsymbol{X}(q,p)\} + \sum_{q=1}^{M} Re\{\boldsymbol{\Upsilon}(q,q)\boldsymbol{X}(q,q)\}. \tag{26}$$

Because the positions of BS and RIS are generally fixed, the transmission paths between BS and RIS are pre-known. As a consequence, the steering vector $\boldsymbol{a}(\boldsymbol{\zeta}_{RI})$ is fixed. In addition, we assume that the distance between BS and RIS is much longer than the element spacing in RIS, based on which we have $\theta_i = \theta_{i,m}, \varphi_i = \varphi_{i,m}, \forall m \in M$. Then, we define

$$\psi_y = \cos\theta_i \sin\varphi_i, \tag{27}$$

$$\psi_z = \sin\theta_i. \tag{28}$$

The spatial information incident at the m-th element of RIS can be sequentially expressed as

$$\boldsymbol{\zeta}_{RI,m} = (m_y - 1)\psi_y + (m_z - 1)\psi_z. \tag{29}$$

Additionally, we assume that the element spacing equals half wavelength, i.e., $d = \frac{\lambda}{2}$. Then, for the URA case, $\boldsymbol{\Upsilon}(p,q)$ as the function of θ_{lb}, θ_{ub}, φ_{lb}, and φ_{ub} can be expressed as

$$\boldsymbol{\Upsilon}(p,q) = \frac{\int_{\theta_{lb}}^{\theta_{ub}} \int_{\varphi_{lb}}^{\varphi_{ub}} e^{j\pi\iota} d\varphi d\theta}{(\theta_{ub} - \theta_{lb})(\varphi_{ub} - \varphi_{lb})}, \tag{30}$$

where $\iota = [(p_y - q_y)(\cos\theta\sin\varphi + \psi_y) + (p_z - q_z)(\sin\theta + \psi_z)]$. Note that the direct integral of the angle ranges will be challenging, especially when both θ and φ are variables. We then discuss the average received power Ξ in the following three special cases:

A. When $\theta_{o,l,m}$ is a fixed value, $\varphi_{o,l,m} \in (-90°, 90°)$, $m = 1, \cdots, M$:

Assume that the elevation angle $\theta_{o,l,m}$ is fixed to be a constant angle $\overline{\theta}$, then (6) can be rewritten as

$$\zeta_{RO,l,m} = (m_y - 1)\cos\overline{\theta}\sin(\varphi_{o,l,m}) + (m_z - 1)\sin\overline{\theta}. \tag{31}$$

As the direct integral over the angle $\varphi_{o,l,m}$ can be challenging, we map $\tau_{lb} = \sin(\varphi_{lb})$ and $\tau_{ub} = \sin(\varphi_{ub})$, and the variable τ follows uniform distribution over the pre-defined cover region in terms of $[\tau_{lb}, \tau_{ub}]$. Then, the certain element $\boldsymbol{\Upsilon}(p,q)$ can be approximated as [28]

$$\boldsymbol{\Upsilon}(p,q) = \frac{\int_{\tau_{lb}}^{\tau_{ub}} A_p A_q^H \, d\tau}{\tau_{ub} - \tau_{lb}}, \tag{32}$$

where $A_{\{i=p,q\}} = e^{j\pi(\zeta_{RI,i} + \zeta_{RO,i})}$.

Moreover, $\zeta_{RO,i}$ originated from (31), l is eliminated as the continuous integral is considered over the cover region $[\tau_{lb}, \tau_{ub}]$ in (32). We expand the integral term, and (32) can be further expressed as

$$\boldsymbol{\Upsilon}(p,q) = \begin{cases} \xi, & p_y = q_y, \\ \frac{e^{j\pi(p_y - q_y)\cos\overline{\theta}\tau_{ub}} - e^{j\pi(p_y - q_y)\cos\overline{\theta}\tau_{lb}}}{j\pi(p_y - q_y)(\tau_{ub} - \tau_{lb})\cos\overline{\theta}}\xi, & p_y \neq q_y, \end{cases} \tag{33}$$

where $\xi = e^{j\pi[(p_y - q_y)\psi_y + (p_z - q_z)(\sin\overline{\theta} + \psi_z)]}$.

When the full cover of the azimuth angle from $-90°$ to $90°$ is considered, i.e., $\tau_{lb} = -1$ and $\tau_{ub} = 1$, it should be noticed that

$$\boldsymbol{\Upsilon}(p,q) = \frac{\sin(\pi(p_y - q_y)\cos\overline{\theta})}{\pi(p_y - q_y)\cos\overline{\theta}} \cdot \xi, \tag{34}$$

when $p_y \neq q_y$. Particularly, when the elevation angle $\overline{\theta} = 0$, we have

$$\boldsymbol{\Upsilon}(p,q) = \begin{cases} e^{j\pi(p_z - q_z)\psi_z}, & p_y = q_y, \\ 0, & p_y \neq q_y. \end{cases} \tag{35}$$

Then, the average received power Ξ could be expressed as

$$\Xi = \sum_{p_y = q_y} \boldsymbol{\Upsilon}(p,q)\boldsymbol{X}(q,p). \tag{36}$$

From (23), we can get that M_z elements in each row of $\boldsymbol{Q}_l \in \mathbb{C}^{M_y M_z \times M_y M_z}$ meet the condition $p_y = q_y$. Therefore, there are $M_y M_z^2$ elements in $\boldsymbol{\Upsilon} = \mathbb{E}\{\boldsymbol{Q}_l\}$ satisfying $\boldsymbol{\Upsilon}(p,q) \neq 0$. The following corollary can be sequentially obtained.

$$\boldsymbol{Q}_l = \begin{bmatrix} \gamma_{l,11}\gamma_{l,11}^H & \cdots & \gamma_{l,11}\gamma_{l,1M_z}^H & \cdots & \gamma_{l,11}\gamma_{l,q_yq_z}^H & \cdots & \gamma_{l,11}\gamma_{l,M_y1}^H & \cdots & \gamma_{l,11}\gamma_{l,M_yM_z}^H \\ \vdots & \ddots & & & & & & & \vdots \\ \gamma_{l,1M_z}\gamma_{l,11}^H & \cdots & \gamma_{l,1M_z}\gamma_{l,1M_z}^H & \cdots & \gamma_{l,1M_z}\gamma_{l,q_yq_z}^H & \cdots & \gamma_{l,1M_z}\gamma_{l,M_y1}^H & \cdots & \gamma_{l,1M_z}\gamma_{l,M_yM_z}^H \\ \vdots & & & \ddots & & & & & \vdots \\ \gamma_{l,p_yp_z}\gamma_{l,11}^H & \cdots & \gamma_{l,p_yp_z}\gamma_{l,1M_z}^H & \cdots & \gamma_{l,p_yp_z}\gamma_{l,q_yq_z}^H & \cdots & \gamma_{l,p_yp_z}\gamma_{l,M_y1}^H & \cdots & \gamma_{l,p_yp_z}\gamma_{l,M_yM_z}^H \\ \vdots & & & & & \ddots & & & \vdots \\ \gamma_{l,M_y1}\gamma_{l,11}^H & \cdots & \gamma_{l,M_y1}\gamma_{l,1M_z}^H & \cdots & \gamma_{l,M_y1}\gamma_{l,q_yq_z}^H & \cdots & \gamma_{l,M_y1}\gamma_{l,M_y1}^H & \cdots & \gamma_{l,M_y1}\gamma_{l,M_yM_z}^H \\ \vdots & & & & & & & \ddots & \vdots \\ \gamma_{l,M_yM_z}\gamma_{l,11}^H & \cdots & \gamma_{l,M_yM_z}\gamma_{l,1M_z}^H & \cdots & \gamma_{l,M_yM_z}\gamma_{l,q_yq_z}^H & \cdots & \gamma_{l,M_yM_z}\gamma_{l,M_y1}^H & \cdots & \gamma_{l,M_yM_z}\gamma_{l,M_yM_z}^H \end{bmatrix}, \tag{23}$$

Corollary 1: *The upper bound of the average received power is reached when* $w_{m_y,m_z} = e^{j\pi m_z\psi_z}$. *The upper bound across the azimuth domain denoted as* $\hat{\Xi}_\varphi$ *can be obtained as*

$$\hat{\Xi}_\varphi = M_y M_z^2. \tag{37}$$

To be noted, the integral is taken over the mapped sin function τ of the directions, as the direct integral over $\varphi_{o,l,m}$ can be challenging. The variable chosen criterion is to find sufficient random directions which are non-overlapping and could well represent the pre-defined cover region. Indeed, integrals taken over the mapped sin function τ and the direction φ by applying the Riemann sum approximation method [29] result in the same average received power. See proof in APPENDIX A.

B. When $\varphi_{o,l,m}$ is fixed, $\theta_{o,l,m} \in (-90°, 90°)$, $m = 1, \cdots, M$:

Assume that $\varphi_{o,l,m}$ is fixed as $\varphi_{o,l,m} = \overline{\varphi}$, then (6) can be rewritten as

$$\zeta_{RO,l,m} = (m_y - 1)\cos(\theta_{o,l,m})\sin\overline{\varphi} + (m_z - 1)\sin(\theta_{o,l,m}). \tag{38}$$

We define $\nu_{ub} = \sin(\theta_{o,ub})$ and $\nu_{lb} = \sin(\theta_{o,lb})$, which contains the phase information of the boundary of the cover region. Similar to (32), we can get the expression for a certain element in $\boldsymbol{\Upsilon}(p,q)$ as

$$\boldsymbol{\Upsilon}(p,q) = \frac{\int_{\nu_{lb}}^{\nu_{ub}} Z_p \cdot Z_q \, d\nu}{\nu_{ub} - \nu_{lb}}, \tag{39}$$

where $Z_{\{i=p,q\}} = e^{j\pi((p_y-1)(\pm\sqrt{1-\nu^2}\sin\overline{\varphi}+\psi_y)+(p_z-1)(\nu+\psi_z))}$.

As the integral can be challenging to solve analytically, we assume $\overline{\varphi} = 0$. Then $\boldsymbol{\Upsilon}$ is further discussed considering the relationship between p_z and q_z. We firstly have

$$\boldsymbol{\Upsilon}(p,q) = \begin{cases} \varrho, & p_z = q_z, \\ \frac{e^{j\pi(p_z-q_z)\nu_{ub}} - e^{j\pi(p_z-q_z)\nu_{lb}}}{j\pi(p_z-q_z)(\nu_{ub}-\nu_{lb})}\varrho, & p_z \neq q_z, \end{cases} \tag{40}$$

where $\varrho = e^{j\pi((p_y-q_y)\psi_y+(p_z-q_z)\psi_z)}$.

By introducing the full cover of the elevation angle from $-90°$ to $90°$, i.e., $\nu_{lb} = -1$ and $\nu_{ub} = 1$, $\boldsymbol{\Upsilon}(p,q)$ can be rewritten as

$$\boldsymbol{\Upsilon}(p,q) = \begin{cases} e^{j\pi((p_y-q_y)\psi_y+(p_z-q_z)\psi_z)}, & p_z = q_z, \\ 0, & p_z \neq q_z. \end{cases} \tag{41}$$

Furthermore, from (23), we observe that in each column of $\boldsymbol{Q}_l$, there are M_y elements satisfying $p_z = q_z$. In total, there should be $M_y^2 M_z$ elements meeting the $p_z = q_z$ condition in $\boldsymbol{\Upsilon} = \mathbb{E}\{\boldsymbol{Q}_l\}$. With fixed azimuth angle $\overline{\varphi} = 0$, the average received power Ξ with $\theta_{o,m} \in (-90°, 90°)$ can be expressed as

$$\Xi = \sum_{p_z=q_z} \boldsymbol{\Upsilon}(p,q)\boldsymbol{X}(q,p). \tag{42}$$

Based on the derivation, we get a corollary, as shown below.

Corollary 2: *The upper bound of the average power across the elevation domain* $\hat{\Xi}_\theta$ *as*

$$\hat{\Xi}_\theta = M_y^2 M_z, \tag{43}$$

which is achieved when $w_{m_y,m_z} = e^{j\pi(m_y\psi_y+m_z\psi_z)}$.

C. When $M_x = 1$ or $M_y = 1$:

The designed URA configuration is transferred in the ULA model with either $M_x = 1$ or $M_y = 1$. In the case of ULA, we give the following analysis and derivation regarding the average received power.

When ULA configuration is applied, (6) can be rewritten as

$$\zeta_{RO,l,m} = (m-1)\sin(\phi_{o,l,m}), \tag{44}$$

where $\phi_{o,l,m}$ denotes the steering angle towards the l-th direction in the ULA model, and $m = 1, \cdots, M$. And we further define $\psi_{\text{ULA}} = \sin\theta_i$. Regarding to (32) and (39), $\boldsymbol{\Upsilon}(p,q)$ can be expressed as

$$\boldsymbol{\Upsilon}(p,q) = \frac{\int_{\mu_{lb}}^{\mu_{ub}} e^{j\pi(p-1)(\mu+\psi_{\text{ULA}})} e^{-j\pi(q-1)(\mu+\psi_{\text{ULA}})} \, d\mu}{\mu_{ub} - \mu_{lb}}, \tag{45}$$

which could be further rewritten as

$$\boldsymbol{\Upsilon}(p,q) = \begin{cases} 1, & p = q, \\ \frac{e^{j\pi(p-q)\mu_{ub}} - e^{j\pi(p-q)\mu_{lb}}}{j\pi(p-q)(\mu_{ub}-\mu_{lb})} e^{j\pi(p-q)\psi_{\text{ULA}}}, & p \neq q. \end{cases} \tag{46}$$

Note that $\mu = sin(\phi_{o,l,m})$. μ_{ub} and μ_{lb} contain the phase information of boundaries of the cover region. Since both $\boldsymbol{\Upsilon}$ and $\boldsymbol{X}$ are Hermitian matrices, we can easily get that

$$\sum_{q=1}^{M} Re\{\boldsymbol{\Upsilon}(q,q)\boldsymbol{X}(q,q)\} = M, \tag{47}$$

based on which we rewrite (26) as

$$\Xi = 2\sum_{p=1}^{M}\sum_{q=p+1}^{M} Re\{\boldsymbol{\Upsilon}(p,q)\boldsymbol{X}(q,p)\} + M. \tag{48}$$

According to (46) and (48), we can derive the following corollary.

Corollary 3: *The average received power within a specific range from μ_{lb} to μ_{ub} could be expressed as*

$$\Xi = M + 2\sum_{p=1}^{M-1}\sum_{q=p+1}^{M} Re\{w_q w_p^* \frac{e^{j\pi(p-q)\mu_{ub}} - e^{j\pi(p-q)\mu_{lb}}}{j\pi(p-q)(\mu_{ub}-\mu_{lb})} e^{j\pi(p-q)\psi_{\text{ULA}}}\}, \tag{49}$$

where the average received power is a function of the cover region boundaries μ_{lb} and μ_{ub}, the incident angle information ψ_{ULA}, and the RIS phase shifts $\mathbf{w}$.

Specially, when full cover from $\phi = -90°$ to $90°$ is considered, i.e., $\mu_{lb} = -1$ and $\mu_{ub} = 1$, we have

$$\frac{e^{j\pi(p-q)\mu_{ub}} - e^{j\pi(p-q)\mu_{lb}}}{j\pi(p-q)(\mu_{ub}-\mu_{lb})} = 0, \tag{50}$$

when $p \neq q$. By taking (50) into (49), we can henceforth get the theorem as shown below.

Theorem 1: *When full cover from RIS is considered, the average received power $\Xi_{ULA} = M$ can be realized regardless of the phase shifts configuration of RIS.*

When other sizes of cover area are considered, the maximum average received power, and its corresponding RIS phase shifts cannot be mathematically derived. We, therefore, aim to find an upper bound of the average received power that an arbitrary cover region could realise.

Based on **Theorem 1**, we can get the sum power receiving from RIS as

$$\Xi_{total} = \int_{-1}^{1} \Xi_{ULA} d\mu = 2M. \tag{51}$$

It is noted that the sum power is calculated based on dimensionless values of trigonometric functions and henceforth is with no unit. Since the average received power within a pre-defined target region is aimed to be maximized, we take the value $\hat{\Xi}_{ULA}$ obtained when the beams are all within this range as the upper bound of the average power, i.e., there are no side lobes in other areas. Note that no side lobes might be impractical in the real application; however, the side lobes could be significantly suppressed by some beamforming designs such as MRT and the beam broadening technique addressed in [23]. Then the upper bound of the average received power $\hat{\Xi}_{ULA}$ as a function of the angular range can be interpreted as

$$\hat{\Xi}_{ULA} = \frac{2M}{\mu_{ub} - \mu_{lb}}, \quad \mu_{ub} - \mu_{lb} \in (0, 2]. \tag{52}$$

The derived upper bound of the received power can be effectively used as the benchmark to evaluate the amount of the power reflecting to the pre-defined angular region. Following this, we get a corollary shown below.

Corollary 4: *The range of the upper bound for an arbitrary pre-defined cover region could be derived as*

$$\hat{\Xi}_{ULA} \in [M, M^2]. \tag{53}$$

To be noted, when the length of the range tends to zero, the upper bound average received power is not obtained by (52). In detail, the derivation can be seen in APPENDIX B.

We further assume that there is a specific cover range $[\phi_a, \phi_b]$, whose corresponding determined sinusoidal range is $[\mu_a, \mu_b]$, where $\mu_a = \sin\phi_a$ and $\mu_b = \sin\phi_b$. Its maximum average received power Ξ_{ab} is realized when RIS's phase shift is $\boldsymbol{\alpha}^* \in \mathbb{C}^{M\times 1}$, which can not be mathematically derived in close-form but can be obtained by some optimization algorithms such as interior method [30], etc. Specifically, the m-th phase shift in RIS is α_m^*. Another cover region which has the same sinusoidal range as $[\mu_a, \mu_b]$ is denoted as $[\phi_a', \phi_b']$, where its corresponding sinusoidal range is set as $[\mu_a + \Delta, \mu_b + \Delta]$. Δ is defined as the sinusoidal difference between ϕ_a/ϕ_b and ϕ_a'/ϕ_b', which should be within the range $\Delta \in [-1 - \mu_a, 1 - \mu_b]$. Furthermore, we define the same difference of these sinusoidal ranges as $\overline{\zeta}$, where $\overline{\zeta} = \mu_b - \mu_a$. The following theorem can be derived.

Theorem 2: *The same maximum average received power can always be realized by RIS phase shift regardless of the orientation of the cover region as long as the sinusoidal difference $\overline{\zeta}$ is equal. However, when the cover region is shifted to be near the cover boundaries, the power pattern will degrade compared with the pattern which points to the centre angle by using only the phase information of the weight.*
The proof can be seen in APPENDIX C.

As an important metric that characterises the generated broadbeam's performance, we derive the maximum average received power within a specific sector area on the communication system. These numerical results can serve as a baseline for evaluating the concentration of signals' power within the specific cover region.

IV. DC-SDP ALGORITHM

In this section, we investigate the solutions for the RIS-aided flat broad beamwidth design proposed in Section II based on the maximum average received power derived in Section III. The DC-SDP algorithm, which effectively addresses the non-convexity issue while keeping the unit modulus characteristic of RIS weights, is introduced.

In (P1), we aim to maximize the average received power within an arbitrary pre-defined angular region while all users in that region could receive signals with the same power. To proceed, we choose a set of uniformly distributed directions $\{1, 2, \cdots, L\} \in [\upsilon_{lb}, \upsilon_{ub}]$ under both ULA and URA configuration.

Additionally, it is proved that for an arbitrary ULA, when only one element is with unit power while others are zero, the perfect flat broadbeam can be realized [31]. It can also be easily verified in the case of URA configuration. This perfect broadbeam design with only one active element obviously violates the unit modulus principle regarding RIS weights. To achieve a flat beam design, we henceforth introduce δ to characterize the fluctuation of the generated broadbeam. Then, our optimization problem could be re-interpreted as

$$\begin{aligned} \text{(P2):} \quad \max_{\mathbf{w}} \quad & \Xi \\ \text{s.t.} \quad & p_l = \Xi + \delta, \quad l = 1, 2, \cdots, L \\ & |\delta| \leq \delta_{max}, \\ & |w_m| = 1, \quad m = 1, \cdots, M. \end{aligned} \tag{54}$$

where a small fluctuation $0 < |\delta| \ll 1$ is tolerable and is designed to be smaller than δ_{max}.

Furthermore, we assume that the users are in the vicinity of the RIS while far from the BS. Therefore, we rewrite $\boldsymbol{h}_{d,l} = \boldsymbol{h}_d, l = 1, \cdots, L$, and sequentially, we have $\boldsymbol{h}_d^H \boldsymbol{b}\sqrt{p_t} = \hat{h_d}$ and $\boldsymbol{G}\boldsymbol{b}\sqrt{p_t} = \hat{\boldsymbol{g}} \in \mathbb{C}^{M\times 1}$. Then, the received power at the l-th direction can be expressed as

$$p_l \approx |\hat{h_d} + \boldsymbol{h}_{r,l}^H \boldsymbol{W} \hat{\boldsymbol{g}}|^2 + \sigma_n^2. \tag{55}$$

We define $\boldsymbol{\eta}_l = \text{diag}(\boldsymbol{h}_{r,l}^H)\hat{\boldsymbol{g}} \in \mathbb{C}^{M\times 1}$, then (55) is transformed as

$$p_l = \mathbf{w}^H \boldsymbol{C}_l \mathbf{w} + 2Re\{\mathbf{w}^H \boldsymbol{u}_l\} + |\hat{h_d}|^2 + \sigma_n^2, \tag{56}$$

where $\boldsymbol{C}_l = \boldsymbol{\eta}_l \boldsymbol{\eta}_l^H \in \mathbb{C}^{M\times M}$, and $\boldsymbol{u}_l = \boldsymbol{\eta}_l^H \hat{h_d} \in \mathbb{C}^{M\times 1}$. We further let $\boldsymbol{R}_l = \begin{bmatrix} \boldsymbol{C}_l & \boldsymbol{u}_l \\ \boldsymbol{u}_l^H & 0 \end{bmatrix}$ and $\overline{\mathbf{w}} = \begin{bmatrix} \mathbf{w} \\ 1 \end{bmatrix}$, then the received power at the l-th direction can be rewritten as

$$p_l = (\overline{\mathbf{w}}^H \boldsymbol{R}_l \overline{\mathbf{w}}) + |\hat{h_d}|^2 + \sigma_n^2 \tag{57}$$

By introducing $\overline{\mathbf{w}}^H \boldsymbol{R}_l \overline{\mathbf{w}} = \text{Tr}(\boldsymbol{R}_l \overline{\boldsymbol{W}})$, where $\overline{\boldsymbol{W}} = \overline{\mathbf{w}}\overline{\mathbf{w}}^H$, the problem (P2) can be henceforth reformulated as a standard SDP problem [32] without loss of generality:

$$\begin{aligned} \text{(P3):} \quad \max_{\overline{\boldsymbol{W}}} \quad & \Xi \\ \text{s.t.} \quad & \text{Tr}(\boldsymbol{R}_l \overline{\boldsymbol{W}}) + |\hat{h_d}|^2 + \sigma_n^2 = \Xi + \delta, l = 1, \cdots, L \\ & |\delta| \le \delta_{max}, \\ & \overline{\boldsymbol{W}}_{m,m} = 1, \quad m = 1, \cdots, M+1, \\ & \text{rank}(\overline{\boldsymbol{W}}) = 1, \\ & \overline{\boldsymbol{W}} \succeq 0, \end{aligned} \tag{58}$$

Note that problem (P3) is a non-convex optimization problem due to the rank-one constraint. Instead of simply dropping the rank-one condition or relaxing the strict unit modulus weights constraint, we rewrite the rank-one constraint into an equivalent form:

$$\text{rank}(\overline{\boldsymbol{W}}) = 1 \Longleftrightarrow \text{Tr}(\overline{\boldsymbol{W}}) - \|\overline{\boldsymbol{W}}\|_2 = 0, \tag{59}$$

which can be considered as the difference between the two convex functions. Specifically, $\text{Tr}(\overline{\boldsymbol{W}}) = \sum_{i=1}^{M+1} \sigma_i(\overline{\boldsymbol{W}})$ and $\|\overline{\boldsymbol{W}}\|_2 = \sigma_1(\overline{\boldsymbol{W}})$, where $\sigma_i(\overline{\boldsymbol{W}})$ denotes the i-th largest singular value of matrix $\overline{\boldsymbol{W}}$. From $\text{Tr}(\overline{\boldsymbol{W}}) = \|\overline{\boldsymbol{W}}\|_2$, we can easily indicate that all singular values equal 0 except the largest one, equivalently, the rank-one constraint can be met.

Unfortunately, problem (P3) is still non-convex in terms of $\overline{\boldsymbol{W}}$ when substituting the rank-one constraint by (59), given the fact that $-\|\overline{\boldsymbol{W}}\|_2$ is a concave term. In order to solve the non-convexity issue, a penalty-based method is firstly invoked by adding the penalty component into the objective function in problem (P3), yielding

$$\begin{aligned} \text{(P4):} \quad \min_{\overline{\boldsymbol{W}}} \quad & -\Xi + \rho(\text{Tr}(\overline{\boldsymbol{W}}) - \|\overline{\boldsymbol{W}}\|_2) \\ \text{s.t.} \quad & \text{Tr}(\boldsymbol{Q}_l \overline{\boldsymbol{W}}) + |\hat{h_d}|^2 + \sigma_n^2 = \Xi + \delta, l = 1, \cdots, L \\ & |\delta| \le \delta_{max}, \\ & \overline{\boldsymbol{W}} \succeq 0, \\ & \overline{\boldsymbol{W}}_{m,m} = 1, \quad m = 1, \cdots, M+1, \end{aligned} \tag{60}$$

where ρ is the penalty factor and should satisfy $\rho > 0$.

Note that the non-convexity issue is not fully addressed since the concave term $-\rho\|\overline{\boldsymbol{W}}\|_2$ still exists. However, our objective function is now in a standard difference-of-convex (DC) form. We, therefore, use the DC algorithm, where the successive cancellation algorithm (SCA) approach can be developed to construct a convex function at the specific point in each iteration based on the original non-convex objective function. Then the proposed problem can be iterative-optimized, where a convex problem is formulated in each iteration.

For simplicity, we firstly focus on the term $\text{Tr}(\overline{\boldsymbol{W}}) - \|\overline{\boldsymbol{W}}\|_2$, and define

$$g(\overline{\boldsymbol{W}}) = \text{Tr}(\overline{\boldsymbol{W}}), \tag{61}$$

$$h(\overline{\boldsymbol{W}}) = \|\overline{\boldsymbol{W}}\|_2. \tag{62}$$

Then, we have a new objective function

$$\min \quad F(\overline{\boldsymbol{W}}) = g(\overline{\boldsymbol{W}}) - h(\overline{\boldsymbol{W}}). \tag{63}$$

According to Fenchel's duality theorem that

$$\begin{aligned} \alpha &= \inf\{g(\boldsymbol{Y}) - h(\boldsymbol{Y}) : \boldsymbol{Y} \in \mathcal{Y}\} \\ &= \inf\{g(\boldsymbol{Y}) - \sup\{\langle \boldsymbol{Y}, \boldsymbol{Z}\rangle - h^*(\boldsymbol{Z}) : \boldsymbol{Z} \in \mathcal{Y}\} : \boldsymbol{Y} \in \mathcal{Y}\} \\ &= \inf\{\beta(\boldsymbol{Z}) : \boldsymbol{Z} \in \mathcal{Z}\} \end{aligned} \tag{64}$$

where

$$\beta(\boldsymbol{Z}) = \begin{cases} h^*(\boldsymbol{Z}) - g^*(\boldsymbol{Z}), & \boldsymbol{Z} \in \text{domain } h^*, \\ +\infty, & \text{otherwise}, \end{cases} \tag{65}$$

we can directly optimize the objective function through the following algorithm without considering the constraint functions in problem (P4).

Algorithm 1 DC algorithm for IRR

Input: $\boldsymbol{Y}^0$.
Output: $\boldsymbol{Y}^K$.
1: **for** $t = 0 : K-1$ **do**
2: $\quad \boldsymbol{Z}^t = \partial h_{\boldsymbol{Y}^t}(\boldsymbol{Y})$;
3: $\quad \boldsymbol{Y}^{t+1} \in \text{arginf}\{g(\boldsymbol{Y}) - h(\boldsymbol{Y}^t) - \langle \boldsymbol{Y} - \boldsymbol{Y}^t, \boldsymbol{Z}^t\rangle\}$;
4: **end for**

It can be seen that an affine majorization is applied to the concave part $-h(\overline{\boldsymbol{W}})$. The sub-gradient of the PSD matrix $\mathbf{Y}$ at $\boldsymbol{Y}^t$ can be obtained via $\partial\|\boldsymbol{A}\|_2 = v_1 v_1^H$, where v_1 is the leading eigenvector of matrix $\boldsymbol{A}$. Then, we use singular value decomposition (SVD) technique [33] to decompose matrix $\boldsymbol{A}$ into $\boldsymbol{A} = \boldsymbol{U}\boldsymbol{S}\boldsymbol{V}^H$, where the singular values in $\boldsymbol{S}$ are in decreasing order. Therefore, the most leading eigenvector is $\boldsymbol{U}(:,1)$, i.e., $v_1 = \boldsymbol{U}(:,1)$.

Based on Algorithm 1, the objective function (63) can be equivalently rewritten as

$$F = \text{Tr}(\overline{\boldsymbol{W}}) - \langle \overline{\boldsymbol{W}} - \overline{\boldsymbol{W}}^{t-1}, \partial_{\overline{\boldsymbol{W}}^{t-1}} \|\overline{\boldsymbol{W}}\|_2 \rangle, \tag{66}$$

in the t^{th} iteration, where $\|\overline{\boldsymbol{W}}^{t-1}\|_2$ is ignored since it is a fixed value. To be noted, (66) is a convex function. We can,

Algorithm 2 Proposed DC-SDP algorithm for RIS-aided broadbeam generation

Input: $\boldsymbol{R}_l \in \mathbb{C}^{(M+1)\times(M+1)}, l = 1, \cdots, L$, $\overline{\boldsymbol{W}}^0 \in \mathbb{C}^{(M+1)\times(M+1)}$, $\hat{h_d}$.
Output: $\mathbf{w} \in \mathbb{C}^{M\times 1}$, p_l, $l = 1, 2, \ldots, L$.
for $t = 1 : K$ **do**
Obtain $\overline{\boldsymbol{W}}^t$ and $-\Xi^t + \rho \cdot F^t$ by solving problem (P5) using CVX toolbox;
$[\boldsymbol{U}, \boldsymbol{S}, \boldsymbol{V}] = \text{svd}(\overline{\text{W}}^t)$;
$\partial_{\overline{\boldsymbol{W}}^t} \|\overline{\boldsymbol{W}}\|_2 = \boldsymbol{U}(:, 1)\boldsymbol{U}(:, 1)'$;
Identify the convergence status by (68);
if $C \le \varsigma$ **then**
BREAK
end if
end for
$[\boldsymbol{U}, \boldsymbol{S}, \boldsymbol{V}] = \text{svd}(\overline{\boldsymbol{W}}^t)$.
$\boldsymbol{S} \longrightarrow \overline{\boldsymbol{S}}$ and get e_1.
Obtain $\overline{\mathbf{U}}$ by (69).
Obtain $\overline{\mathbf{w}}$ by (70), and obtain $\mathbf{w}$ by $\mathbf{w} = \overline{w}_{1:M}$.
Obtain p_l by (9), where $l = 1, 2, \ldots, L$.

therefore, formulate problem (P4) into the following convex programming:

$$\begin{aligned} \text{(P5):} \quad \min_{\overline{\boldsymbol{W}}} \quad & -\Xi + \rho \cdot F \\ \text{s.t.} \quad & \text{Tr}(\boldsymbol{R}_l \overline{\boldsymbol{W}}) + |\hat{h_d}|^2 + \sigma_n^2 = \Xi + \delta, l = 1, \cdots, L \\ & |\delta| \le \delta_{max}, \\ & \overline{\boldsymbol{W}} \succeq 0, \\ & \overline{\boldsymbol{W}}_{m,m} = 1, \quad m = 1, \cdots, M+1. \end{aligned} \tag{67}$$

In each iteration, the original SDP problem is transformed into a standard convex optimization problem, which can be efficiently solved by CVX toolbox [34]. After K^{th} iteration, we obtain the optimized $\overline{\boldsymbol{W}}$ corresponding to the objective function with minimized value. The iteration can also be interrupted if the convergence reaches, which could be expressed as

$$C = \Xi^{t-1} - \Xi^t + \rho \cdot (F^t - F^{t-1}) \le \varsigma. \tag{68}$$

Note that ς is the threshold that indicates when the optimization reaches convergence and is then interrupted. After iterative optimization, however, $\text{Tr}(\overline{\boldsymbol{W}}) - \|\overline{\boldsymbol{W}}\|_2$ might be infinitely close to zero, denoting a quasi-rank one matrix $\overline{\boldsymbol{W}}$. Therefore SVD technique is adopted to decompose the PSD matrix $\overline{\boldsymbol{W}}$ into $\overline{\boldsymbol{W}} = \boldsymbol{U}\boldsymbol{S}\boldsymbol{V}^H$, where $\boldsymbol{V}^H$ is the Hermitian transpose of $\boldsymbol{U}$. By remaining the largest non-zero eigenvalue e_1 in $\boldsymbol{S}$, which could be much larger than all other eigenvalues, and forcing others as zero, a new approximated eigenvalue matrix $\overline{\boldsymbol{S}}$ is formed, which can be expressed as $\overline{\mathbf{S}} = [e_1, 0, \cdots, 0]^T \in \mathbb{C}^{(M+1)\times 1}$. We define

$$\overline{\boldsymbol{U}} = [\boldsymbol{U}(:, r)]_{r=1,\cdots,R}, \tag{69}$$

where r depends on the number of non-zero elements in $\overline{\mathbf{S}}$. It can be easily derived that $R = 1$. Finally, we could get the expression of $\overline{\mathbf{w}}$ as

$$\overline{\mathbf{w}} = e^{j\angle(\sqrt{\overline{\boldsymbol{U}}e_1})}/\overline{w}_{M+1}, \tag{70}$$

TABLE I: Simulation Parameters.

Parameters	Values
BS location (in meters)	(0, 0, 10)
RIS location (in meters)	(1000, 0, 10)
Path-loss for $\boldsymbol{G}$ and $\boldsymbol{h}_{r,l}$ (in dB)	$35.6 + 22.0lg(d)$
Path-loss for $\boldsymbol{h}_{d,l}$ (in dB)	$32.6 + 36.7lg(d)$
Transmit power	30 dBm
Noise power	-117 dBm

where $\sqrt{\overline{\boldsymbol{U}}e_1} \in \mathbb{C}^{(M+1)\times 1}$ and $\overline{\mathbf{w}} \in \mathbb{C}^{(M+1)\times 1}$ correspondingly. $\overline{w}_{M+1}$ denotes the $(M+1)$-th element of $\overline{\mathbf{w}}$. The RIS phase shifts $\mathbf{w}$ can be obtained by extracting the first M elements from $\overline{\mathbf{w}}$, i.e., $\mathbf{w} = \overline{w}_{1:M}$.

The entire algorithm is summarized in Algorithm 2. Specifically, $\overline{\boldsymbol{W}}^0$ represents the initialized PSD matrix. The proposed problem (P5) is a standard convex programming, which gradually and monotonously converges through iterative optimization and eventually becomes stable. We henceforth get RIS phase shifts $\mathbf{w}$, which enable flat broadbeam in a pre-defined cover area.

V. Simulation results

In this section, numerical results are provided to evaluate the performance of our proposed algorithm. We first clarify the simulation parameters, followed by a numerical analysis of the sum rate under different beamforming designs. Then, simulations are demonstrated to verify our derivation in Section III. As important indicators of iterative algorithms, the complexity and convergence of our proposed algorithm are analyzed. Furthermore, the power patterns under the practical channel model are simulated under both ULA and URA configurations.

A. Simulation Scenario

We assume a scenario placed in an x-y-z Cartesian coordinate system, where a 2×2 antennas BS located at $(0, 0)$m, with a height of 10m, and a single RIS is implemented in the vicinity of users to provide high-quality reflective links between the BS and users. Specifically, the RIS's location is at $(1000, 0, 10)$m, with a distance of 1000m to the BS. Moreover, considering the orientation of BS and RIS, we let $\varphi_n = 30°$, $\theta_n = -60°$, $n = 1, \cdots, N$, and $\varphi_{i,m} = -30°$, and $\theta_{i,m} = 60°, m = 1, \cdots, M$ under URA configuration. The cover range at the reflecting side of RIS with a radius of 10m is studied. The L chosen directions are uniform-distributed in both elevation and azimuth domains. Under ULA configuration, we assume the distance between BS and RIS is 1000m as well. The AoD at BS is set as 60°, and the AoA at RIS is −60°. As the direct links are severely blocked and only NLoS paths exist, we consider MRT beamforming at BS towards the RIS for maximal power transmission. The detailed simulation parameters refer to [35] and are given in Table 1. Specifically, we assume the carrier frequency is 2.4 GHz, and the path-loss of channels is set according to the 3GPP propagation environment. Furthermore, we set the element spacing distance at the BS and the RIS as $d = \lambda/2$. The noise power has a spectral density of −170 dBm/Hz. We assume the transmission bandwidth is 200 kHz; therefore, the noise power is about $\sigma_n^2 = -117$ dBm. Additionally, unless stated

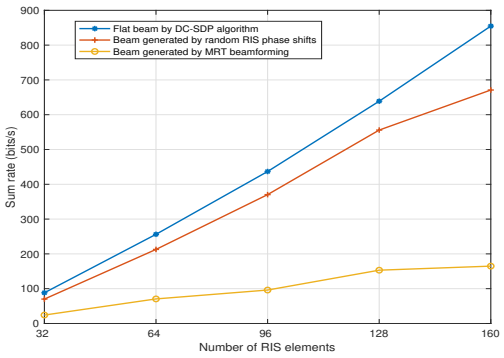

Fig. 3: Investigation of sum rate for different generated beams.

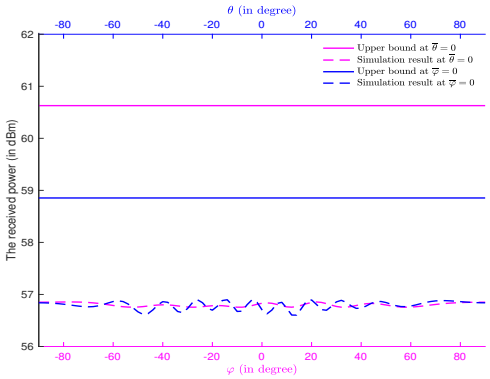

Fig. 4: Comparison between the derived upper bound and the simulation results with flat broadbeam design.

otherwise, we assume $L = M$, and the Rician factor has been set to $\varepsilon = 10$. All the simulation results are averaged over 1000 independent realizations of channel small-scale fading. The tolerated fluctuation of the power pattern, i.e., the variance, is set to be $\delta = 0.01$ dB. The penalty component ρ is set as 100. The iteration interruption threshold is set as $\varsigma = 10^{-4}$. We initialize $\overline{\mathbf{w}}^0 \in \mathbb{C}^{(M+1)\times 1}$ a randomly generated unit-modulus complex vector, then $\overline{\boldsymbol{W}}^0 = \overline{\mathbf{w}}^0(\overline{\mathbf{w}}^0)^H$. Furthermore, we denote the maximum number of iterations as $K = 100$.

B. The sum rate analysis

To illustrate the maximum sum rate property of the flat broadbeam, we compare the sum rate of the flat broadbeam with other generated beams under the same system model. Specifically, the sum rates of the full cover case are compared under different sizes of RIS. The simulation results are shown in Fig. 3. It can be seen that the flat broadbeam design could always realize the highest sum rate compared with the beam generated by other RIS beamforming designs. For example, when the number of RIS elements is $M = 160$, the sum rate realized by the flat broadbeam, the beam generated by random RIS phase shifts, and the beam generated by MRT directional beamforming is 854.69, 670.96, and 164.79 bits/s, respectively.

C. Proof of the derivation under ULA and URA configuration

According to **Corollary 1** and **Corollary 2**, where the upper bounds of the average received power are obtained when $\overline{\theta} = 0$ and $\overline{\varphi} = 0$, respectively. In order to highlight the differences between these two cases, we consider a RIS in URA configuration where $M_x \neq M_y$. Specifically, we have $M_x = 8$ and $M_y = 12$. We consider the full cover case, where the cover region is uniformly divided into $L = 90$ sub-areas in either azimuth or elevation domain, and the angle of each sub-area is 2°. The flat broadbeam design is then investigated. Fig. 4 shows the derived upper bounds and the simulation results at $\overline{\theta} = 0$ and $\overline{\varphi} = 0$. Flat beam patterns with subtle fluctuation are obtained. Additionally, it can be seen that there is not much difference between the simulation results and the theoretical upper limit. Specifically, there is approximately a 4 dB difference when $\overline{\theta} = 0$ and a 2 dB difference when $\overline{\varphi} = 0$, which indicates that the proposed flat broadbeam design is with high energy efficiency.

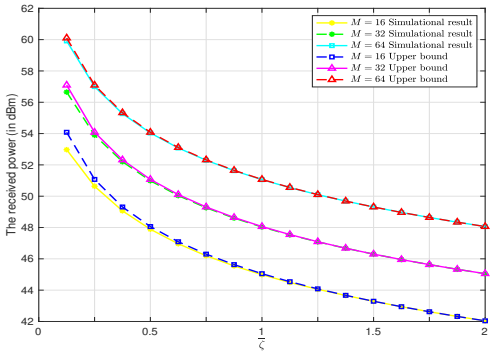

Fig. 5: Comparison of the simulated and theoretical average received power.

Based on **Corollary 3**, we have mathematically verified that when $\lambda/2$-spaced RIS is used, the average gain improvement in all directions is dependent on RIS's size, i.e., $\Xi = M$. We also derive the upper bound of the average received power within an arbitrary angular region, which is dependent on both the size of RIS and the size of the cover region.

In Fig. 5, we compare the simulated maximum average received power versus the upper bound $\hat{\Xi}_{ULA}$ when different angular regions are set. RIS with 16, 32 and 64 elements are used, and the sinusoidal difference $\overline{\zeta} = \mu_{ub} - \mu_{lb}$, which is defined in Section. III, is set to be $\{1/8, 1/4, \cdots, 15/8, 2\}$, corresponding to different pre-defined angular regions. It can be seen that our optimal solutions, considering both the flatness and average received power of the broadbeam, are always close to the upper bound regardless of the size of the RIS, revealing that the side lobe power is limited. Particularly, when the full cover is considered, our optimal solution reaches the same as the upper bound, which is in accordance with **Theorem 1**.

D. Analysis of the DC-SDP algorithm

In this part, we first give an analysis of the complexity and convergence of our proposed algorithm. Then, we compare the DC-SDP algorithm with other state-of-the-art.

Firstly, the complexity of initializing $\boldsymbol{R}_l$, $l = 1, \cdots, L$ is $O(L(M^2 + M))$. According to [36], the complexity of an SDP problem to optimize an $n \times n$ PSD matrix with m SDP constraints in each iteration is given by $O(\sqrt{n}log(1/\epsilon)(mn^3 + m^2n^2 + m^3))$, where $\epsilon > 0$ is the solution accuracy. Therefore,

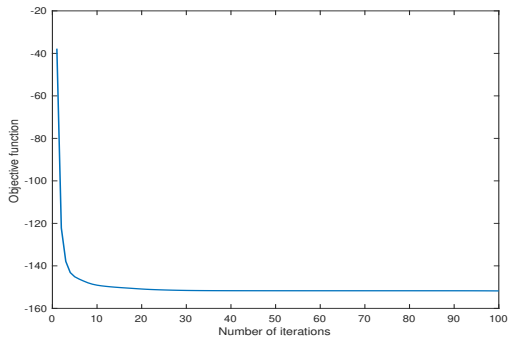

Fig. 6: Proof of convergence of the proposed algorithm.

the complexity of the iterative optimization is approximately $O(log(1/\epsilon)\min\{K, t_{BREAK}\}(L+2)((M+1)^3+L(M+1)^{2.5}))$, where K denotes the maximum number of iterations and t_{BREAK} denotes the number of iterations when convergence reaches. The singular value decomposition of the obatined semi-definite matrix $\overline{\boldsymbol{W}}^t$ has the complexity of $O((M+1)^3)$. In conclusion, our proposed algorithm has the complexity of $O(L(M^2+M)+log(1/\epsilon)\min\{K, t_{BREAK}\}(L+2)((M+1)^3+L(M+1)^{2.5})+(M+1)^3)$.

On the other side, since both the objective function and the constraints are convex, the value of the objective function is non-increasing after each iteration by applying the DC-SDP algorithm. Furthermore, the objective function possesses a finite lower bound due to the principle of energy conservation, which restricts the received power from exceeding its limit. Fig. 6 verifies the convergence of our proposed algorithm numerically, from which we can see that the objective function converges rapidly within the limited number of iterations.

In addition, we compare our broadbeam design with the matching method proposed in [22], the alternating direction method of multipliers (ADMM) algorithm proposed in [37], and also with the cases when either no RIS is implemented or when the RIS is randomly designed. Both the average received power and the variance are presented. Particularly, for the ULA model, we optimize the average received power and the variance over the full cover range from $\phi = -90°$ to $90°$ with RIS composed of $M = 32$, 64, 96, 128, and 160 elements. It can be seen from Fig. 7 that a higher average received power could always be realized with the help of RIS. As the full cover is considered, the RIS beamforming design mainly influences the variance of the beam pattern, while the average received power could be similar. In detail, our proposed algorithm results in a variance lower than 10^{-2} dB, while all other beamforming designs lead to higher variance and more severe fluctuation of the generated broadbeam. For the URA configuration model, the RIS with 2×16, 4×16, 6×16, 8×16, and 10×16 elements are implemented, respectively. We set the target region with the azimuth angle $\varphi \in [-90°, 90°]$ and the elevation angle $\theta \in [-30°, 30°]$. By proposing our developed DC-SDP algorithm, the highest received power could be realized within the pre-defined angular region. On the other side, the variance is minimized to be less than 10^{-2} dB, revealing a perfect flat broadbeam within the cover region.

E. The performance of the proposed algorithm with practical channel model

In this subsection, the power pattern is simulated under both ULA and URA configurations. In detail, the power pattern with different sizes of RIS and different sizes of pre-defined angular regions are investigated. Furthermore, we consider the full cover over the spatial domain, and symmetrical and unsymmetrical pre-defined angular regions are also considered when the region of interest is not the whole spatial domain.

1) The power pattern under ULA configuration

Fig. 8a demonstrates the power pattern under different numbers of RIS elements. We use the RIS composed of $M = 32$, 64, 96, 128, and 160 elements, respectively. The full cover $\phi \in [-90°, 90°]$ is considered. Specifically, the average received power under different sizes of RIS is -109.37, -105.23, -103.49, -102.12, and -101.03 dBm, while the corresponding variance of each power pattern is 0.0025, 0.0064, 0.0032, 0.0023, and 0.0022 dB, respectively. The variance results are lower than the threshold $\delta = 0.01$ dB, revealing the good flatness of the generated power pattern.

Fig. 8b shows the power pattern when different sizes of the pre-defined angular region are considered. A RIS with 180 elements is applied. It is worth mentioning that the side lobes are given in the simulation. Specifically, when the cover region is $\phi = [-45°, 45°]$, the average power of the side lobes is -113.39 dBm, while the average received power of directions within the pre-defined angular region is -98.04 dBm, which is 15.35 dB higher than the average power within the side lobes area. Moreover, when $\phi = [-30°, 30°]$, the average received power within the region of interest is -96.38 dBm, which is 17.52 dB higher than the average power outside the target region. In addition, when the cover region is set to be $\phi = [-15°, 15°]$, the average received power within and outside the target region is -93.51 dBm and -115.86 dBm, respectively. It is found that there is 22.35 dB higher average received power within $\phi \in [-15°, 15°]$ compared with the power within the sidelobe. At the same time, the beam within the region of interest is significantly flattened, with power variance lower than the threshold. In addition, the power patterns when the cover region is not symmetrical are also presented, as it could be a common and practical scenario that needs to be considered. When the target cover region is $\phi \in [-60°, -30°]$, the average received power within and outside the target region is -93.23 and -114.10 dBm, respectively. When the target cover region is $\phi \in [30°, 60°]$, the average received power within and outside the target region is -93.08 and -115.92 dBm, respectively. The variances of the regions of interest are also lower than the threshold, revealing good flatness. It can be seen that our proposed algorithm is robust regardless the shift of the cover range.

Fig. 8c shows the power pattern under different Rician factors when a RIS with $M = 64$ elements is applied. The full cover within $\phi = [-90°, 90°]$ is considered. Specifically, when the Rician factor is $\varepsilon = \{2, 4, 6, 8\}$, the corresponding average received power are -106.59, -106.18, -106.13, -106.89 dBm, and the variances of the power pattern are 0.0024, 0.0041, 0.0058, and 0.0023 dB, respectively. Note

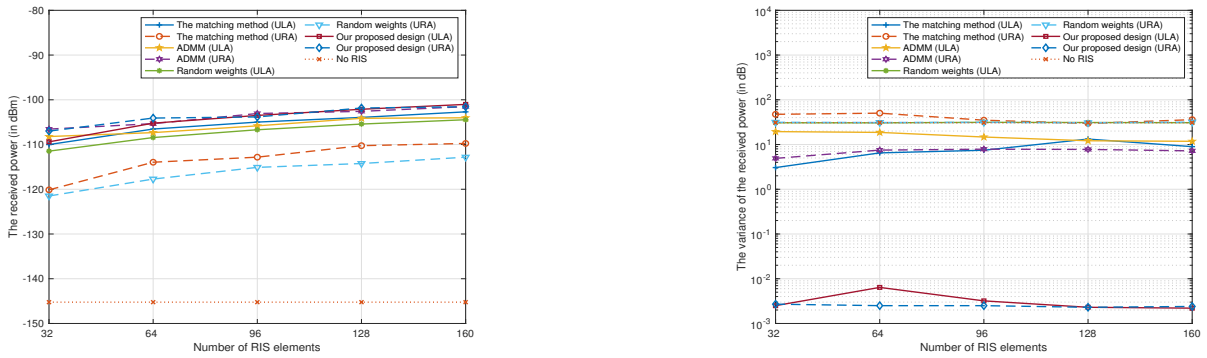

(a) The comparison of the average received power.

(b) The comparison of the variance of the power pattern.

Fig. 7: The comparison under both ULA and URA configurations.

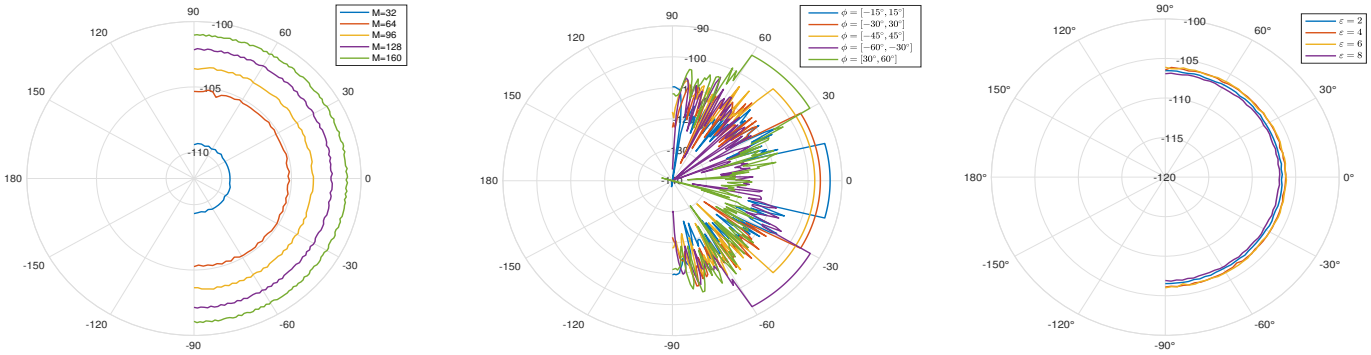

(a) The power pattern with different numbers of RIS elements.

(b) The power pattern with different pre-defined angular regions.

(c) The power pattern with different Rician factor ε.

Fig. 8: The power pattern under practical channel model when ULA configuration is applied.

that this simulation is generated with instantaneous channel state information (CSI), as the average over channel fading could weaken the effects of the Rician factor. The generated broadbeams reveal that our proposed DC-SDP algorithm is robust against various channel environments.

2) The power pattern under URA configuration

Specifically, a RIS with 16×16 elements is applied to generate the flat broadbeam to cover the pre-defined angular region. Fig. 9a presents the power pattern when the pre-defined angular region is across $\theta \in [-30°, 30°]$ and $\varphi \in [-30°, 30°]$. In detail, the average received power within the target region is -96.97 dBm, and the power pattern is flattened with a variance of only 0.0024 dB. On the other side, the average received power towards other angles is only -121.95 dBm, which is about 25 dB lower than the average power received in the target region. Furthermore, Fig. 9b shows the unsymmetrical power pattern when the pre-defined angular region is across $\theta \in [-90°, -30°]$ and $\varphi \in [-30°, 30°]$. The average received power and the variance within the specific range are -95.53 dBm and 0.0025 dB, respectively. At the same time, the average received power at other angles is -113.34 dBm. It is worth mentioning that our proposed DC-SDP algorithm can optimize the flat beam towards arbitrary angular regions in the 3D space. Fig. 9c shows the full cover in both the elevation and azimuth domain. In detail, the average received power among all directions is -102.31 dBm with a variance of only 0.0021 dB. To be noted, when the RIS with the same number of elements is applied, URA configuration will result in a higher sidelobe level compared with ULA model, as directions in both azimuth and elevation domains need to be considered. In order to realize the sidelobe suppression under URA configuration without sacrificing the resolution, a larger RIS or multi-RISs need to be applied.

VI. Conclusion

In this paper, we investigate a RIS-assisted downlink communication system, where a RIS is deployed to generate a flat broadbeam in any pre-defined angular region without known CSI or feedback mechanism. We mathematically derive the expression of the maximum average received power that could be achieved in a cover region with arbitrary size. The upper bound of the average received power is obtained as well. We propose a broad beamwidth design where the average received power is maximized and a restricted fluctuation is allowed in the beam pattern by optimizing RIS phase shifts. To address this non-convex problem, the DC-SDP algorithm is applied. Simulation results verify our proposed theoretical findings and indicate the superiority of the DC-SDP algorithm in generating broadbeam with the best flatness. This application is of great value to be implemented in practical industrial and daily scenarios with low computation and hardware requirements while realizing a high sum rate. Additionally, it can also

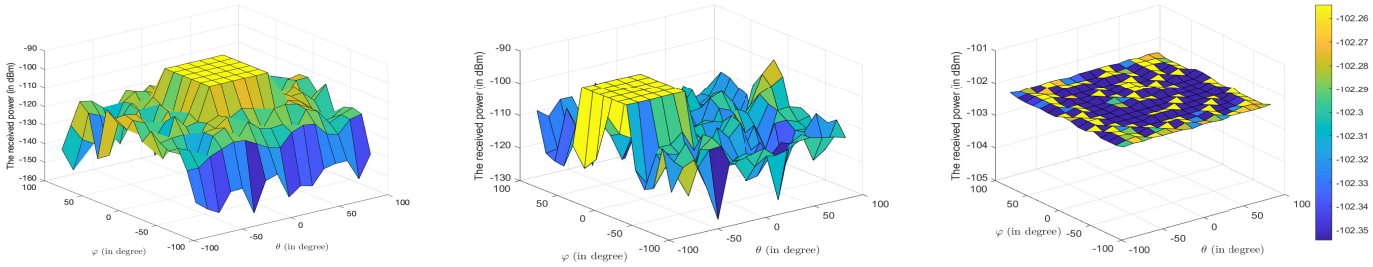

(a) The symmetrical power pattern with $\theta \in [-30°, 30°], \varphi \in [-30°, 30°]$.

(b) The unsymmetrical power pattern with $\theta \in [-90°, -30°], \varphi \in [-30°, 30°]$.

(c) The full cover power pattern.

Fig. 9: The 3D power pattern under URA configuration.

be viewed as the premise of obtaining accurate CSI and establishing communication connections.

Appendix A
Integral approximation by Riemann sum method

Consider the fixed elevation angle $\overline{\theta}$, the (p,q)-th element $\Upsilon(p,q)$ in terms of the variable φ can be expressed as

$$\Upsilon(p,q) = \frac{\int_{\varphi_{lb}}^{\varphi_{ub}} A_p A_q^H \, d\varphi}{\varphi_{ub} - \varphi_{lb}}. \tag{71}$$

As it is challenging to integral over φ directly, we apply the Riemann sum. The main idea of the Riemann sum is to obtain an approximation of a region's area by adding up the areas of multiple simplified slices of the region. Specifically, we divide the azimuth range from φ_{lb} to φ_{ub} into n_a sub-intervals, where each sub-interval has a range of $\Delta\varphi = \frac{\varphi_{ub}-\varphi_{lb}}{n_a}$. A larger number of sub-intervals n_a is desired for a more accurate approximation result. Then (71) can be approximated as

$$\Upsilon(p,q) = \frac{e^{j\pi((p_y-q_y)\psi_y+(p_z-q_z)\psi_z)}}{\varphi_{ub}-\varphi_{lb}} \cdot \sum_{t_1=1}^{n_a} e^{j\pi((p_y-q_y)\cos\overline{\theta}\sin(\varphi_{lb}+\frac{2t_1-1}{2}\Delta\varphi)+(p_z-q_z)\sin\overline{\theta})}\Delta\varphi. \tag{72}$$

Particularly, when the elevation angle $\overline{\theta} = 0$, and the full cover from $\varphi_{lb} = -90°$ to $\varphi_{ub} = 90°$ is considered, (72) can be rewritten as

$$\Upsilon(p,q) = \frac{e^{j\pi((p_y-q_y)\psi_y+(p_z-q_z)\psi_z)}}{n_a} \sum_{t_1=1}^{n_a} e^{j\pi(p_y-q_y)\sin(-\frac{\pi}{2}+\frac{2t_1-1}{2n_a}\pi)}. \tag{73}$$

By considering $p_y = q_y$ and $p_y \neq q_y$ cases, Υ can be explained as

$$\Upsilon(p,q) = \begin{cases} e^{j\pi(p_z-q_z)\psi_z}, & p_y = q_y, \\ 0, & p_y \neq q_y. \end{cases} \tag{74}$$

The result is consistent with (35). Sequentially, **Corollary 1** can be obtained, verifying the feasibility of deriving the average received power by taking integral over the mapped sin function. **Corollary 2** and **Corollary 3** can be similarly derived by taking integral over the angles with the Riemann sum approximation method, which are omitted here due to the page limitation.

Appendix B
Proof of Corollary 4

From (52), it can be seen that $\hat{\Xi}_{ULA}$ is inversely proportional to the difference of the sinusoidal function of the area angle range, i.e., $\mu_{ub} - \mu_{lb}$. However, the received power can not be infinitely large when $\mu_{ub} - \mu_{lb} \to 0$ considering the limited transmitted power at BS as well as the limited size of RIS. We henceforth further investigate the maximum average received power that could be realized in a cover area and rewrite the expression for the average received power as (75). To be noted, $\alpha_m, m = 1, \cdots, M$ is the phase shift of RIS's elements.

From (75) we can indicate that

$$\Xi = M + 2\sum_{p=1}^{M-1}\sum_{q=p+1}^{M} \cos(\alpha_q - \alpha_p + \pi(p-q)(\frac{\mu_{ub}+\mu_{lb}}{2} + \psi_{\text{ULA}})), \tag{76}$$

when $\mu_{ub} - \mu_{lb} \to 0$, given the fact that $\sin(x)/x = 1$ when $x \to 0$. For an extremely small cover area, i.e., $\mu_{ub} - \mu_{lb} \to 0$, $\hat{\Xi}_{max} = M^2$ can be realized through careful designing of RIS phase shifts as

$$\alpha_m = \pi m(\frac{\mu_{ub}+\mu_{lb}}{2} + \psi_{\text{ULA}}), m = 1, 2, \cdots, M. \tag{77}$$

Therefore, **Corollary 4** can be obtained.

Appendix C
Proof of Theorem 2

Given that the optimal RIS phase shifts is $\boldsymbol{\alpha}^* \in \mathbb{C}^{M\times 1}$ when the sinusoidal range of the cover area is $[\mu_a, \mu_b]$, the average received power for the range $[\mu_a + \Delta, \mu_b + \Delta]$ can be then expressed as

$$\Xi' = M + 4\sum_{p=1}^{M-1}\sum_{q=p+1}^{M} \cos(\alpha_q{}' - \alpha_p{}' + \pi(p-q)(\frac{\mu_b+\mu_a+2\Delta}{2} + \psi_{\text{ULA}}))\chi, \tag{78}$$

where

$$\chi = \frac{\sin(\pi(p-q)\frac{\overline{\zeta}}{2})}{\pi(q-p)\overline{\zeta}}. \tag{79}$$

Note that α'_p and α'_q denote the p and q-th phase shift in RIS when the cover range is $[\mu_a + \Delta, \mu_b + \Delta]$. It can be seen that χ keeps the same when $\overline{\zeta}$ is unchanged. Therefore we mainly

$$
\begin{aligned}
\Xi &= M + 2\sum_{p=1}^{M-1}\sum_{q=p+1}^{M} \frac{Re\{(\cos(\alpha_q-\alpha_p)+j\sin(\alpha_q-\alpha_p))e^{j\pi(p-q)(\frac{\mu_{ub}+\mu_{lb}}{2}+\psi_{\mathrm{ULA}})}(e^{j\pi(p-q)\frac{\mu_{ub}-\mu_{lb}}{2}}-e^{-j\pi(p-q)\frac{\mu_{ub}-\mu_{lb}}{2}})\}}{j\pi(p-q)(\mu_{ub}-\mu_{lb})} \\
&= M + 4\sum_{p=1}^{M-1}\sum_{q=p+1}^{M} \frac{Re\{(j\cos(\alpha_q-\alpha_p)-\sin(\alpha_q-\alpha_p))e^{j\pi(p-q)(\frac{\mu_{ub}+\mu_{lb}}{2}+\psi_{\mathrm{ULA}})}\sin(\pi(p-q)\frac{\mu_{ub}-\mu_{lb}}{2})\}}{j\pi(p-q)(\mu_{ub}-\mu_{lb})} \\
&= M + 4\sum_{p=1}^{M-1}\sum_{q=p+1}^{M} \frac{Re\{(\cos(\alpha_q-\alpha_p)+j\sin(\alpha_q-\alpha_p))e^{j\pi(p-q)(\frac{\mu_{ub}+\mu_{lb}}{2}+\psi_{\mathrm{ULA}})}\sin(\pi(q-p)\frac{\mu_{ub}-\mu_{lb}}{2})\}}{\pi(q-p)(\mu_{ub}-\mu_{lb})} \\
&= M + 4\sum_{p=1}^{M-1}\sum_{q=p+1}^{M} \frac{(\cos(\alpha_q-\alpha_p)\cos(\pi(p-q)(\frac{\mu_{ub}+\mu_{lb}}{2}+\psi_{\mathrm{ULA}}))-\sin(\alpha_q-\alpha_p)\sin(\pi(p-q)(\frac{\mu_{ub}+\mu_{lb}}{2}+\psi_{\mathrm{ULA}}))sin(\pi(q-p)\frac{\mu_{ub}-\mu_{lb}}{2})}{\pi(q-p)(\mu_{ub}-\mu_{lb})} \\
&= M + 4\sum_{p=1}^{M-1}\sum_{q=p+1}^{M} \frac{\cos(\alpha_q-\alpha_p+\pi(p-q)(\frac{\mu_{ub}+\mu_{lb}}{2}+\psi_{\mathrm{ULA}}))\sin(\pi(q-p)\frac{\mu_{ub}-\mu_{lb}}{2})}{\pi(q-p)(\mu_{ub}-\mu_{lb})}.
\end{aligned}
\tag{75}
$$

focus on the term $\cos(\alpha_q{}'-\alpha_p{}'+\pi(p-q)(\frac{\mu_{ub}+\Delta+\mu_{lb}+\Delta}{2}+\psi_{\mathrm{ULA}}))$. When

$$\alpha_q{}' = \alpha_q{}^* + \pi q\Delta, \tag{80}$$

and

$$\alpha_p{}' = \alpha_p{}^* + \pi p\Delta, \tag{81}$$

the maximum average received power $\Xi_{ab}{}' = \Xi_{ab}$ is realized. We can get the general expression of the RIS phase shift as

$$\alpha'_m = \alpha^*_m + \pi m\Delta, m = 1, \cdots, M. \tag{82}$$

As a consequence, there will always exist a group of RIS phase shifts $\boldsymbol{\alpha}'$ satisfying (82), such that the maximum average received power for the range $[\mu_a+\Delta, \mu_b+\Delta]$ is the same as that for the range $[\mu_a, \mu_b]$. However, consider that the shape of the broad beam will be hard to be optimized when the target cover region is at the boundary of the area where the RIS can cover, such as cover regions centred at $\pm 80°$, and the side lobes will be hard to be suppressed, the same maximum power is therefore hard to achieve. **Theorem 2** is obtained.

References

[1] R. Prasad, *OFDM for Wireless Communications Systems*. Artech House, 2004.

[2] T. L. Marzetta, "Massive MIMO: An Introduction," *Bell Labs Technical Journal*, vol. 20, pp. 11–22, 2015.

[3] Y. Saito, Y. Kishiyama, A. Benjebbour, T. Nakamura, A. Li, and K. Higuchi, "Non-orthogonal Multiple Access (NOMA) for Cellular Future Radio Access," in *2013 IEEE 77th vehicular technology conference (VTC Spring)*. IEEE, 2013, pp. 1–5.

[4] Q. Wu and R. Zhang, "Intelligent Reflecting Surface Enhanced Wireless Network: Joint Active And Passive Beamforming Design," in *2018 IEEE Global Communications Conference (GLOBECOM)*. IEEE, 2018, pp. 1–6.

[5] T. Kürner and S. Priebe, "Towards THz Communications-status in Research, Standardization and Regulation," *Journal of Infrared, Millimeter, and Terahertz Waves*, vol. 35, no. 1, pp. 53–62, 2014.

[6] H. Xu, L. Zhang, E. Sun *et al.*, "BE-RAN: Blockchain-enabled RAN with Decentralized Identity Management and Privacy-Preserving Communication," *arXiv e-prints*, pp. arXiv–2101, 2021.

[7] Q. Wu, S. Zhang, B. Zheng, C. You, and R. Zhang, "Intelligent Reflecting Surface Aided Wireless Communications: A Tutorial," *IEEE Transactions on Communications*, 2021.

[8] Y. Liu, L. Zhang, B. Yang, W. Guo, and M. A. Imran, "Programmable Wireless Channel for Multi-User MIMO Transmission Using Meta-Surface," in *2019 IEEE Global Communications Conference (GLOBECOM)*, 2019, pp. 1–6.

[9] C. Liaskos, S. Nie, A. Tsioliaridou, A. Pitsillides, S. Ioannidis, and I. Akyildiz, "A New Wireless Communication Paradigm through Software-Controlled Metasurfaces," *IEEE Communications Magazine*, vol. 56, no. 9, pp. 162–169, 2018.

[10] J. Rains, J. U. R. Kazim, L. Zhang, A. Tukmanov, Q. H. Abbasi, and M. A. Imran, "2.75-Bit Reflecting Unit Cell Design for Reconfigurable Intelligent Surfaces," 2021.

[11] C. Pan, H. Ren, K. Wang, J. F. Kolb, M. Elkashlan, M. Chen, M. Di Renzo, Y. Hao, J. Wang, A. L. Swindlehurst *et al.*, "Reconfigurable Intelligent Surfaces for 6G Systems: Principles, Applications, and Research Directions," *IEEE Communications Magazine*, vol. 59, no. 6, pp. 14–20, 2021.

[12] G. R. Mati, S. Das, and T. Swami, "An Improved Multi-IRS Aided MISO System Using Multivariate Analysis," in *2021 IEEE 18th India Council International Conference (INDICON)*, 2021, pp. 1–6.

[13] Z. Ding and H. V. Poor, "A Simple Design of IRS-NOMA Transmission," *IEEE Communications Letters*, vol. 24, no. 5, pp. 1119–1123, 2020.

[14] J. Chen, Y.-C. Liang, Y. Pei, and H. Guo, "Intelligent Reflecting Surface: A Programmable Wireless Environment for Physical Layer Security," *IEEE Access*, vol. 7, pp. 82 599–82 612, 2019.

[15] D. Xu, X. Yu, Y. Sun, D. W. K. Ng, and R. Schober, "Resource Allocation for IRS-assisted Full-duplex Cognitive Radio Systems," *IEEE Transactions on Communications*, vol. 68, no. 12, pp. 7376–7394, 2020.

[16] Z.-Q. He and X. Yuan, "Cascaded Channel Estimation for Large Intelligent Metasurface Assisted Massive MIMO," *IEEE Wireless Communications Letters*, vol. 9, no. 2, pp. 210–214, 2020.

[17] T. L. Jensen and E. De Carvalho, "An Optimal Channel Estimation Scheme for Intelligent Reflecting Surfaces Based on a Minimum Variance Unbiased Estimator," in *ICASSP 2020 - 2020 IEEE International Conference on Acoustics, Speech and Signal Processing (ICASSP)*, 2020, pp. 5000–5004.

[18] J. Xu, C. Yuen, C. Huang, N. Ul Hassan, G. C. Alexandropoulos, M. Di Renzo, and M. Debbah, "Reconfiguring Wireless Environments via Intelligent Surfaces for 6G: Reflection, Modulation, and Security," *Science China Information Sciences*, vol. 66, no. 3, p. 130304, 2023.

[19] Y. Han, W. Tang, S. Jin, C.-K. Wen, and X. Ma, "Large Intelligent Surface-Assisted Wireless Communication Exploiting Statistical CSI," *IEEE Transactions on Vehicular Technology*, vol. 68, no. 8, pp. 8238–8242, 2019.

[20] Y. Gao, J. Xu, W. Xu, D. W. K. Ng, and M.-S. Alouini, "Distributed IRS With Statistical Passive Beamforming for MISO Communications," *IEEE Wireless Communications Letters*, vol. 10, no. 2, pp. 221–225, 2021.

[21] Y. Sun, K. An, J. Luo, Y. Zhu, G. Zheng, and S. Chatzinotas, "Outage Constrained Robust Beamforming Optimization for Multiuser IRS-Assisted Anti-Jamming Communications With Incomplete Information," *IEEE Internet of Things Journal*, vol. 9, no. 15, pp. 13 298–13 314, 2022.

[22] V. Jamali, G. C. Alexandropoulos, R. Schober, and H. V. Poor, "Low-to-Zero-Overhead IRS Reconfiguration: Decoupling Illumination and Channel Estimation," *IEEE Communications Letters*, vol. 26, no. 4, pp. 932–936, 2022.

[23] H. Lu, Y. Zeng, S. Jin, and R. Zhang, "Aerial Intelligent Reflecting Surface: Joint Placement and Passive Beamforming Design With 3D Beam Flattening," *IEEE Transactions on Wireless Communications*, vol. 20, no. 7, pp. 4128–4143, 2021.

[24] M. He, J. Xu, W. Xu, H. Shen, N. Wang, and C. Zhao, "RIS-Assisted Quasi-Static Broad Coverage for Wideband mmWave Massive MIMO Systems," *IEEE Transactions on Wireless Communications*, pp. 1–1, 2022.

[25] Y. Liu, L. Zhang, and M. A. Imran, "Multi-User Beamforming and Transmission Based on Intelligent Reflecting Surface," *IEEE Transactions on Wireless Communications*, vol. 21, no. 9, pp. 7329–7342, 2022.

[26] L. Di Stefano and S. Mattoccia, "A Sufficient Condition Based on the cauchy-schwarz Inequality for Efficient Template Matching," in *Proceedings 2003 International Conference on Image Processing (Cat. No.03CH37429)*, vol. 1, 2003, pp. I–269.

[27] A. Mobasher, R. Sotirov, and A. K. Khandani, "Matrix-lifting Semi-definite Programming for Detection in Multiple Antenna Systems," *IEEE Transactions on Signal Processing*, vol. 58, no. 10, pp. 5178–5185, 2010.

[28] X. Liu and D. Qiao, "Location-fair Beamforming For High Speed Railway Communication Systems," *IEEE Access*, vol. 6, pp. 28 632–28 642, 2018.

[29] V. Sealey, "Definite integrals, Riemann sums, and area under a curve: What is necessary and sufficient," in *Proceedings of the 28th annual meeting of the North American Chapter of the International Group for the Psychology of Mathematics Education*, vol. 2, no. 1991. Citeseer, 2006, pp. 46–53.

[30] H. Laamari, J. Belfiore, and N. Ibrahim, "Near Maximum Likelihood Detection Using an Interior Point Method and Semidefinite Programming," in *Conference Record of the Thirty-Eighth Asilomar Conference on Signals, Systems and Computers, 2004.*, vol. 1, 2004, pp. 223–226 Vol.1.

[31] D. Qiao, H. Qian, and G. Y. Li, "Broadbeam for Massive MIMO Systems," *IEEE Transactions on Signal Processing*, vol. 64, no. 9, pp. 2365–2374, 2016.

[32] J. Xue, X. Zhou, C. Wang, D. Wang, Y. Zhao, and Z. Li, "Hybrid Precoding for IRS-assisted Secure mmWave Communication System with SWIPT," in *2020 International Conference on Space-Air-Ground Computing (SAGC)*. IEEE, 2020, pp. 82–86.

[33] D. Kalman, "A Singularly Valuable Decomposition: The SVD of a Matrix," *The college mathematics journal*, vol. 27, no. 1, pp. 2–23, 1996.

[34] P. D. Tao and L. T. H. An, "Convex Analysis Approach to DC Programming: Theory, Algorithms and Applications," *Acta mathematica vietnamica*, vol. 22, no. 1, pp. 289–355, 1997.

[35] H. Guo, Y.-C. Liang, J. Chen, and E. G. Larsson, "Weighted Sum-Rate Maximization for Reconfigurable Intelligent Surface Aided Wireless Networks," *IEEE Transactions on Wireless Communications*, vol. 19, no. 5, pp. 3064–3076, 2020.

[36] S. Zargari, A. Khalili, Q. Wu, M. Robat Mili, and D. W. K. Ng, "Max-Min Fair Energy-Efficient Beamforming Design for Intelligent Reflecting Surface-Aided SWIPT Systems With Non-Linear Energy Harvesting Model," *IEEE Transactions on Vehicular Technology*, vol. 70, no. 6, pp. 5848–5864, 2021.

[37] Y. Liu, B. Jiu, and H. Liu, "ADMM-based Transmit Beampattern Synthesis for Antenna Arrays under a Constant Modulus Constraint," *Signal Processing*, vol. 171, p. 107529, 2020.